A&A 520, A3 (2010)
DOI: 10.1051/0004-6361/200912837

Astronomy & Astrophysics
Special feature

Pre-launch status of the Planck mission

Planck pre-launch status: The *Planck*-LFI programme

N. Mandolesi[1], M. Bersanelli[2], R. C. Butler[1], E. Artal[7], C. Baccigalupi[8,36,6], A. Balbi[5], A. J. Banday[9,40], R. B. Barreiro[17], M. Bartelmann[9], K. Bennett[27], P. Bhandari[10], A. Bonaldi[3], J. Borrill[38,39], M. Bremer[27], C. Burigana[1], R. C. Bowman[10], P. Cabella[5,46], C. Cantalupo[39], B. Cappellini[2], T. Courvoisier[11], G. Crone[12], F. Cuttaia[1], L. Danese[8], O. D'Arcangelo[13], R. D. Davies[14], R. J. Davis[14], L. De Angelis[15], G. de Gasperis[5], A. De Rosa[1], G. De Troia[5], G. de Zotti[3], J. Dick[8], C. Dickinson[14], J. M. Diego[17], S. Donzelli[22,23], U. Dörl[9], X. Dupac[41], T. A. Enßlin[9], H. K. Eriksen[22,23], M. C. Falvella[15], F. Finelli[1,35], M. Frailis[6], E. Franceschi[1], T. Gaier[10], S. Galeotta[6], F. Gasparo[6], G. Giardino[27], F. Gomez[18], J. Gonzalez-Nuevo[8], K. M. Górski[10,42], A. Gregorio[16], A. Gruppuso[1], F. Hansen[22,23], R. Hell[9], D. Herranz[17], J. M. Herreros[18], S. Hildebrandt[18], W. Hovest[9], R. Hoyland[18], K. Huffenberger[44], M. Janssen[10], T. Jaffe[14], E. Keihänen[19], R. Keskitalo[19,34], T. Kisner[39], H. Kurki-Suonio[19,34], A. Lähteenmäki[20], C. R. Lawrence[10], S. M. Leach[8,36], J. P. Leahy[14], R. Leonardi[21], S. Levin[10], P. B. Lilje[22,23], M. López-Caniego[17,43], S. R. Lowe[14], P. M. Lubin[21], D. Maino[2], M. Malaspina[1], M. Maris[6], J. Marti-Canales[12], E. Martinez-Gonzalez[17], M. Massardi[3], S. Matarrese[4], F. Matthai[9], P. Meinhold[21], A. Melchiorri[46], L. Mendes[24], A. Mennella[2], G. Morgante[1], G. Morigi[1], N. Morisset[11], A. Moss[30], A. Nash[10], P. Natoli[5,37,45,1], R. Nesti[25], C. Paine[10], B. Partridge[26], F. Pasian[6], T. Passvogel[12], D. Pearson[10], L. Pérez-Cuevas[12], F. Perrotta[8], G. Polenta[45,46,47], L. A. Popa[28], T. Poutanen[34,19,20], G. Prezeau[10], M. Prina[10], J. P. Rachen[9], R. Rebolo[18], M. Reinecke[9], S. Ricciardi[1,38,39], T. Riller[9], G. Rocha[10], N. Roddis[14], R. Rohlfs[11], J. A. Rubiño-Martin[18], E. Salerno[48], M. Sandri[1], D. Scott[30], M. Seiffert[10], J. Silk[31], A. Simonetto[13], G. F. Smoot[29,32], C. Sozzi[13], J. Sternberg[27], F. Stivoli[38,39], L. Stringhetti[1], J. Tauber[27], L. Terenzi[1], M. Tomasi[2], J. Tuovinen[33], M. Türler[11], L. Valenziano[1], J. Varis[33], P. Vielva[17], F. Villa[1], N. Vittorio[5,37], L. Wade[10], M. White[49], S. White[9], A. Wilkinson[14], A. Zacchei[6], and A. Zonca[2]

(Affiliations can be found after the references)

Received 6 July 2009 / Accepted 27 October 2009

ABSTRACT

This paper provides an overview of the Low Frequency Instrument (LFI) programme within the ESA *Planck* mission. The LFI instrument has been developed to produce high precision maps of the microwave sky at frequencies in the range 27−77 GHz, below the peak of the cosmic microwave background (CMB) radiation spectrum. The scientific goals are described, ranging from fundamental cosmology to Galactic and extragalactic astrophysics. The instrument design and development are outlined, together with the model philosophy and testing strategy. The instrument is presented in the context of the *Planck* mission. The LFI approach to ground and inflight calibration is described. We also describe the LFI ground segment. We present the results of a number of tests demonstrating the capability of the LFI data processing centre (DPC) to properly reduce and analyse LFI flight data, from telemetry information to calibrated and cleaned time ordered data, sky maps at each frequency (in temperature and polarization), component emission maps (CMB and diffuse foregrounds), catalogs for various classes of sources (the Early Release Compact Source Catalogue and the Final Compact Source Catalogue). The organization of the LFI consortium is briefly presented as well as the role of the core team in data analysis and scientific exploitation. All tests carried out on the LFI flight model demonstrate the excellent performance of the instrument and its various subunits. The data analysis pipeline has been tested and its main steps verified. In the first three months after launch, the commissioning, calibration, performance, and verification phases will be completed, after which *Planck* will begin its operational life, in which LFI will have an integral part.

Key words. cosmic microwave background – space vehicles: instruments – instrumentation: detectors – instrumentation: polarimeters – submillimeter: general – telescopes

1. Introduction

In 1992, the COsmic Background Explorer (COBE) team announced the discovery of intrinsic temperature fluctuations in the cosmic microwave background radiation (CMB; see Appendix A for a list of the acronyms appearing in this paper) on angular scales greater than 7° and at a level of a few tens of μK (Smoot et al. 1992). One year later two spaceborne CMB experiments were proposed to the European Space Agency (ESA) in the framework of the Horizon 2000 scientific programme: the COsmic Background Radiation Anisotropy Satellite (COBRAS; Mandolesi et al. 1994), an array of receivers based on high electron mobility transistor (HEMT) amplifiers; and the SAtellite for Measurement of Background Anisotropies (SAMBA), an array of detectors based on bolometers (Tauber et al. 1994). The two proposals were accepted for an assessment study with the recommendation to merge. In 1996, ESA selected a combined mission called COBRAS/SAMBA, subsequently renamed *Planck*, as the third

Horizon 2000 medium-sized mission. Today *Planck* forms part of the "Horizon 2000" ESA programme.

The *Planck* CMB anisotropy probe[1], the first European and third generation mission after COBE and WMAP (Wilkinson Microwave Anisotropy Probe), represents the state-of-the-art in precision cosmology today (Tauber et al. 2010; Bersanelli et al. 2010; Lamarre et al. 2010). The *Planck* payload (telescope instrument and cooling chain) is a single, highly integrated spaceborne CMB experiment. *Planck* is equipped with a 1.5-m effective aperture telescope with two actively-cooled instruments that will scan the sky in nine frequency channels from 30 GHz to 857 GHz: the Low Frequency Instrument (LFI) operating at 20 K with pseudo-correlation radiometers, and the High Frequency Instrument (HFI; Lamarre et al. 2010) with bolometers operating at 100 mK. Each instrument has a specific role in the programme. The present paper describes the principal goals of LFI, its instrument characteristics and programme. The coordinated use of the two different instrument technologies and analyses of their output data will allow optimal control and suppression of systematic effects, including discrimination of astrophysical sources. All the LFI channels and four of the HFI channels will be sensitive to the linear polarisation of the CMB. While HFI is more sensitive and should achieve higher angular resolution, the combination of the two instruments is required to accurately subtract Galactic emission, thereby allowing a reconstruction of the primordial CMB anisotropies to high precision.

LFI (see Bersanelli et al. 2010, for more details) consists of an array of 11 corrugated horns feeding 22 polarisation-sensitive (see Leahy et al. 2010, for more details) pseudo-correlation radiometers based on HEMT transistors and MMIC technology, which are actively cooled to 20 K by a new concept sorption cooler specifically designed to deliver high efficiency, long duration cooling power (Wade et al. 2000; Bhandari et al. 2004; Morgante et al. 2009). A differential scheme for the radiometers is adopted in which the signal from the sky is compared with a stable reference load at ~4 K (Valenziano et al. 2009). The radiometers cover three frequency bands centred on 30 GHz, 44 GHz, and 70 GHz. The design of the radiometers was driven by the need to minimize the introduction of systematic errors and suppress noise fluctuations generated in the amplifiers. Originally, LFI was to include seventeen 100 GHz horns with 34 high sensitivity radiometers. This system, which could have granted redundancy and cross-calibration with HFI as well as a cross-check of systematics, was not implemented.

The design of the horns is optimized to produce beams of the highest resolution in the sky and the lowest side lobes. Typical LFI main beams have full width half maximum (*FWHM*) resolutions of about 33′, 27′, and 13′, respectively at 30 GHz, 44 GHz, and 70 GHz, slightly superior to the requirements listed in Table 1 for the cosmologically oriented 70 GHz channel. The beams are approximately elliptical with and ellipticity ratio (i.e., major/minor axis) of $\simeq 1.15-1.40$. The beam profiles will be measured in-flight by observing planets and strong radio sources (Burigana et al. 2001).

A summary of the LFI performance requirements adopted to help develop the instrument design is reported in Table 1.

[1] *Planck* (http://www.esa.int/Planck) is a project of the European Space Agency – ESA – with instruments provided by two scientific Consortia funded by ESA member states (in particular the lead countries: France and Italy) with contributions from NASA (USA), and telescope reflectors provided in a collaboration between ESA and a scientific Consortium led and funded by Denmark.

Table 1. LFI performance requirements.

Frequency channel	30 GHz	44 GHz	70 GHz
InP detector technology	MIC	MIC	MMIC
Angular resolution [arcmin]	33	24	14
δT per 30′ pixel [μK]	8	8	8
$\delta T/T$ per pixel [μK/K]	2.67	3.67	6.29
Number of radiometers (or feeds)	4 (2)	6 (3)	12 (6)
Effective bandwidth [GHz]	6	8.8	14
System noise temperature [K]	10.7	16.6	29.2
White noise per channel [$\mu\mathrm{K}\cdot\sqrt{\mathrm{s}}$]	116	113	105
Systematic effects [μK]	<3	<3	<3

Notes. The average sensitivity per 30′ pixel or per $FWHM^2$ resolution element (δT and $\delta T/T$, respectively) is given in CMB temperature units (i.e. equivalent thermodynamic temperature) for 14 months of integration. The white noise (per frequency channel and 1 s of integration) is given in antenna temperature units. See Tables 2 and 6 for LFI measured performance.

The constraints on the thermal behaviour, required to minimize systematic effects, dictated a *Planck* cryogenic architecture that is one of the most complicated ever conceived for space. Moreover, the spacecraft has been designed to exploit the favourable thermal conditions of the L2 orbit. The thermal system is a combination of passive and active cooling: passive radiators are used as thermal shields and pre-cooling stages, while active cryocoolers are used both for instrument cooling and pre-cooling. The cryochain consists of the following main subsystems (Collaudin & Passvogel 1999):

- pre-cooling from 300 K to about 50 K by means of passive radiators in three stages (~150 K, ~100 K, ~50 K), which are called V-Grooves due to their conical shape;
- cooling to 18 K for LFI and pre-cooling the HFI 4 K cooler by means of a H_2 Joule-Thomson cooler with sorption compressors (the sorption cooler);
- cooling to 4 K to pre-cool the HFI dilution refrigerator and the LFI reference loads by means of a helium Joule-Thomson cooler with mechanical compressors;
- cooling of the HFI to 1.6 K and finally 0.1 K with an open loop ^{4}He–^{3}He dilution refrigerator.

The LFI front end unit is maintained at its operating temperature by the *Planck* H_2 sorption cooler subsystem (SCS), which is a closed-cycle vibration-free continuous cryocooler designed to provide 1.2 W of cooling power at a temperature of 18 K. Cooling is achieved by hydrogen compression, expansion through a Joule-Thomson valve and liquid evaporation at the cold stage. The *Planck* SCS is the first long-duration system of its kind to be flown on a space platform. Operations and performance are described in more detail in Sect. 3.3 and in Morgante et al. (2009).

Planck is a spinning satellite. Thus, its receivers will observe the sky through a sequence of (almost great) circles following a scanning strategy (SS) aimed at minimizing systematic effects and achieving all-sky coverage for all receivers. Several parameters are relevant to the SS. The main one is the angle, α, between the spacecraft spin axis and the telescope optical axis. Given the extension of the focal plane unit, each beam centre points to its specific angle, α_r. The angle α is set to be 85° to achieve a nearly all-sky coverage even in the so-called *nominal* SS in which the spacecraft spin axis is kept always exactly along the antisolar direction. This choice avoids the "degenerate" case α_r = 90°, characterized by a concentration of the crossings of scan

circles only at the ecliptic poles and the consequent degradation of the quality of destriping and map-making codes (Burigana et al. 1997; Maino et al. 1999; Wright et al. 1996; Janssen & Gulkis 1992). Since the *Planck* mission is designed to minimize straylight contamination from the Sun, Earth, and Moon (Burigana et al. 2001; Sandri et al. 2010), it is possible to introduce modulations of the spin axis from the ecliptic plane to maximize the sky coverage, keeping the solar aspect angle of the spacecraft constant for thermal stability. This drives us towards the adopted *baseline* SS[2] (Maris et al. 2006a). Thus, the baseline SS adopts a cycloidal modulation of the spin axis, i.e. a precession around a nominal antisolar direction with a semiamplitude cone of 7.5°. In this way, all *Planck* receivers will cover the whole sky. A cycloidal modulation with a 6-month period satisfies the mission operational constraints, while avoiding sharp gradients in the pixel hit count (Dupac & Tauber 2005). Furthermore, this solution allows one to spread the crossings of scan circles across a wide region that is beneficial to map-making, particularly for polarisation (Ashdown et al. 2007). The last three SS parameters are: the sense of precession (clockwise or anticlockwise); the initial spin axis phase along the precession cone; and, finally, the spacing between two consecutive spin axis repointings, chosen to be 2′ to achieve four all-sky surveys with the available guaranteed number of spin axis manoeuvres.

Fifteen months of integration have been guaranteed since the approval of the mission. This will allow us to complete at least two all-sky surveys using all the receivers. The mission lifetime is going to be formally approved for an extension of 12 months, which will allow us to perform more than 4 complete sky surveys.

LFI is the result of an active collaboration between about a hundred universities and research centres, in Europe, Canada, and USA, organized by the LFI consortium (supported by more than 300 scientists) funded by national research and space agencies. The principal investigator leads a team of 26 co-Investigators responsible for the development of the instrument hardware and software. The hardware was developed under the supervision of an instrument team. The data analysis and its scientific exploitation are mostly carried out by a core team, working in close connection with the data processing centre (DPC). The LFI core team is a diverse group of relevant scientists (currently ∼140) with the required expertise in instrument, data analysis, and theory to deliver to the wider *Planck* community the main mission data products. The core cosmology programme of *Planck* will be performed by the LFI and HFI core teams. The core team is closely linked to the wider *Planck* scientific community, consisting, besides the LFI consortium, of the HFI and Telescope consortia, which are organized into various working groups. *Planck* is managed by the ESA *Planck* science team.

The paper is organized as follows. In Sect. 2, we describe the LFI cosmological and astrophysical objectives and LFI's role in the overall mission. We compare the LFI and WMAP sensitivities with the CMB angular power spectrum (APS) in similar frequency bands, and discuss the cosmological improvement from WMAP represented by LFI alone and in combination with HFI. Section 3 describes the LFI optics, radiometers, and sorption cooler set-up and performance. The LFI programme is set forth in Sect. 4. The LFI DPC organisation is presented in Sect. 6, following a report on the LFI tests and verifications in Sect. 5. Our conclusions are presented in Sect. 7.

[2] The above nominal SS is kept as a backup solution in case of a possible verification in-flight of unexpected problems with the *Planck* optics.

2. Cosmology and astrophysics with LFI and *Planck*

Planck is the third generation space mission for CMB anisotropies that will open a new era in our understanding of the Universe (The Planck Collaboration 2006). It will measure cosmological parameters with a much greater level of accuracy and precision than all previous efforts. Furthermore, *Planck*'s high resolution all-sky survey, the first ever over this frequency range, will provide a legacy to the astrophysical community for years to come.

2.1. Cosmology

The LFI instrument will play a crucial role for cosmology. Its LFI 70 GHz channel is in a frequency window remarkably clear from foreground emission, making it particularly advantageous for observing both CMB temperature and polarisation. The two lower frequency channels at 30 GHz and 44 GHz will accurately monitor Galactic and extra-Galactic foreground emissions (see Sect. 2.2), whose removal (see Sect. 2.3) is critical for a successful mission. This aspect is of key importance for CMB polarisation measurements since Galactic emission dominates the polarised sky.

The full exploitation of the cosmological information contained in the CMB maps will be largely based on the joint analysis of LFI and HFI data. While a complete discussion of this aspect is beyond the scope of this paper, in the next few subsections we discuss some topics of particular relevance to LFI or a combined analysis of LFI and HFI data. In Sect. 2.1.1, we review the LFI sensitivity to the APS on the basis of the realistic LFI sensitivity (see Table 6) and resolution (see Table 2) derived from extensive tests. This instrument description is adopted in Sect. 2.1.2 to estimate the LFI accuracy of the extraction of a representative set of cosmological parameters, alone and in combination with HFI. Section 2.1.3 addresses the problem of the detection of primordial non-Gaussianity, a topic of particular interest to the LFI consortium, which will require the combination of LFI and HFI, because of the necessity to clean the foreground. On large angular scales, WMAP exhibits a minimum in the foreground signal in the V band (61 GHz, frequency range 53−69 GHz), thus we expect that the LFI 70 GHz channel will be particularly helpful for investigating the CMB pattern on large scales, a topic discussed in Sect. 2.1.4.

It is important to realise that these are just a few examples of what *Planck* is capable of. The increased sensitivity, fidelity and frequency range of the maps, plus the dramatic improvement in polarisation capability will allow a wide discovery space. As well as measuring parameters, there will be tests of inflationary models, consistency tests for dark energy models, and significant new secondary science probes from correlations with other data-sets.

2.1.1. Sensitivity to CMB angular power spectra

The statistical information encoded in CMB anisotropies, in both temperature and polarisation, can be analyzed in terms of a "compressed" estimator, the APS, C_ℓ (see e.g., Scott & Smoot 2008). Provided that the CMB anisotropies obey Gaussian statistics, as predicted in a wide class of models, the set of C_ℓs contains most of the relevant statistical information. The quality of the recovered power spectrum is a good predictor of

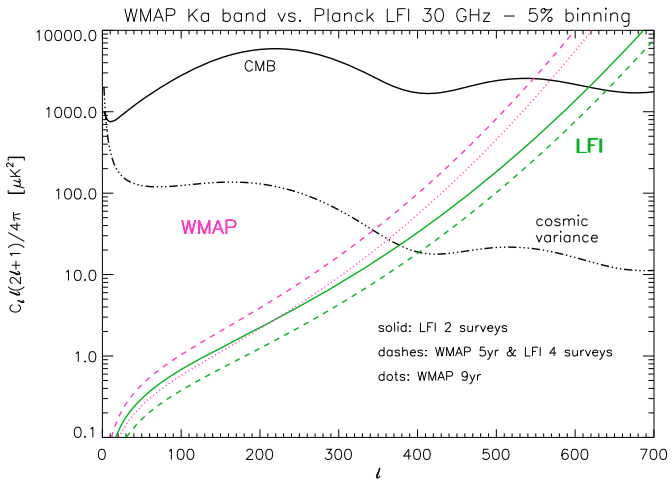

Fig. 1. CMB temperature anisotropy power spectrum (black solid line) compatible with WMAP data is compared to WMAP (Ka band) and LFI (30 GHz) sensitivity, assuming subtraction of the noise expectation, for different integration times as reported in the figure. Two *Planck* surveys correspond to about one year of observations. The plot shows separately the cosmic variance (black three dot-dashes) and the instrumental noise (red and green lines for WMAP and LFI, respectively) assuming a multipole binning of 5%. This binning allows us to improve the sensitivity of the power spectrum estimation. For example, around $\ell = 1000$ (100) this implies averaging the APS over 50 (5) multipoles. Regarding sampling variance, an all-sky survey is assumed here for simplicity. The use of the CAMB code is acknowledged (see footnote 3).

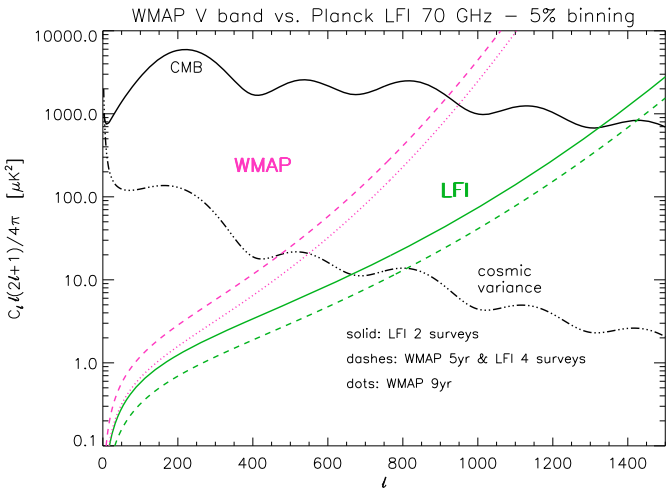

Fig. 2. As in Fig. 1 but for the sensitivity of WMAP in *V* band and LFI at 70 GHz.

the efficiency of extracting cosmological parameters by comparing the theoretical predictions of Boltzmann codes[3]. Strictly speaking, this task must be carried out using likelihood analyses (see Sect. 2.3). Neglecting systematic effects (and correlated noise), the sensitivity of a CMB anisotropy experiment to C_ℓ, at each multipole ℓ, is summarized by the equation (Knox 1995)

$$\frac{\delta C_\ell}{C_\ell} \simeq \sqrt{\frac{2}{f_{\rm sky}(2\ell+1)}}\left[1+\frac{A\sigma^2}{NC_\ell W_\ell}\right], \quad (1)$$

where A is the size of the surveyed area, $f_{\rm sky} = A/4\pi$, σ is the rms noise per pixel, N is the total number of observed pixels, and W_ℓ is the beam window function. For a symmetric Gaussian beam, $W_\ell = \exp(-\ell(\ell+1)\sigma_{\rm B}^2)$, where $\sigma_{\rm B} = FWHM/\sqrt{8\ln 2}$ defines the beam resolution.

Even in the limit of an experiment of infinite sensitivity ($\sigma = 0$), the accuracy in the power spectrum is limited by so-called cosmic and sampling variance, reducing to pure cosmic variance in the case of all-sky coverage. This dominates at low ℓ because of the relatively small number of available modes m per multipole in the spherical harmonic expansion of a sky map. The multifrequency maps that will be obtained with *Planck* will allow one to improve the foreground subtraction and maximize the effective sky area used in the analysis, thus improving our understanding of the CMB power spectrum obtained from previous experiments. However, the main benefits of the improved foreground subtraction will be in terms of polarisation and non-Gaussianity tests.

[3] http://camb.info/

Figures 1 and 2 compare WMAP[4] and LFI[5] sensitivity to the CMB temperature C_ℓ at two similar frequency bands, displaying separately the uncertainty originating in cosmic variance and instrumental performance and considering different project lifetimes. For ease of comparison, we consider the same multipole binning (in both cosmic variance and instrumental sensitivity). The figures show how the multipole region where cosmic variance dominates over instrumental sensitivity moves to higher multipoles in the case of LFI and that the LFI 70 GHz channel allows us to extract information about an additional acoustic peak and two additional throats with respect to those achievable with the corresponding WMAP *V* band.

As well as the temperature APS, LFI can measure polarisation anisotropies (Leahy et al. 2010). A somewhat similar comparison is shown in Figs. 3 and 4 but for the "E" and "B" polarisation modes, considering in this case only the longest mission lifetimes (9 yrs for WMAP, 4 surveys for *Planck*) reported in previous figures and a larger multipole binning (which implies an increase in the signal-to-noise ratio compared to previous figures). Clearly, foreground is more important for measurements of polarisation than for measurements of temperature. In the WMAP *V* band and the LFI 70 GHz channels, the polarised foreground is minimal (at least considering a very large fraction of the sky and for the range of multipoles already explored by WMAP). Thus, we consider these optimal frequencies to represent the potential uncertainty expected from polarised foregrounds. The Galactic foreground dominates over the CMB B mode and also the CMB E mode by up to multipoles of several tens. However, foreground subtraction at an accuracy of 5−10% of the map level is enough to reduce residual Galactic contamination to well below both the CMB E mode and the CMB B mode for a wide range of multipoles for $r = T/S \simeq 0.3$ (here r is defined in Fourier space). If we are able to model Galactic polarised foregrounds with an accuracy at the several percent level, then, for the LFI 70 GHz channel the main limitation will come from instrumental noise. This will prevent an accurate E mode evaluation at $\ell \sim 7$−20, or a B mode detection for $r \lesssim 0.3$. Clearly, a more accurate recovery of the polarisation modes will be possible from the exploitation of the *Planck* data at all frequencies. In this context, LFI data will be crucial

[4] http://lambda.gsfc.nasa.gov/

[5] In this comparison, we exploit realistic LFI optical and instrumental performance as described in the following sections.

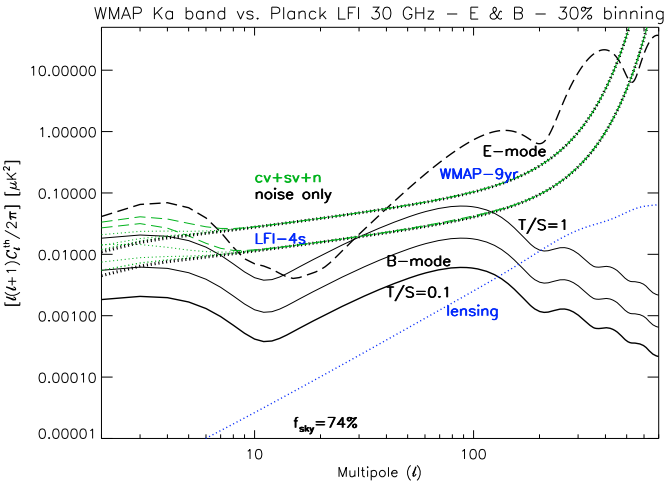

Fig. 3. CMB E polarisation modes (black long dashes) compatible with WMAP data and CMB B polarisation modes (black solid lines) for different tensor-to-scalar ratios of primordial perturbations ($r \equiv T/S = 1, 0.3, 0.1$, at increasing thickness) are compared to WMAP (Ka band, 9 years of observations) and LFI (30 GHz, 4 surveys) sensitivity to the power spectrum, assuming the noise expectation has been subtracted. The plots include cosmic and sampling variance plus instrumental noise (green dots for B modes, green long dashes for E modes, labeled with cv+sv+n; black thick dots, noise only) assuming a multipole binning of 30% (see caption of Fig. 1 for the meaning of binning and of the number of sky surveys). Note that the cosmic and sampling (74% sky coverage; as in WMAP polarization analysis, we exclude the sky regions mostly affected by Galactic emission) variance implies a dependence of the overall sensitivity at low multipoles on r (again the green lines refer to $r = 1, 0.3, 0.1$, from top to bottom), which is relevant to the parameter estimation; instrumental noise only determines the capability of detecting the B mode. The B mode induced by lensing (blue dots) is also shown for comparison.

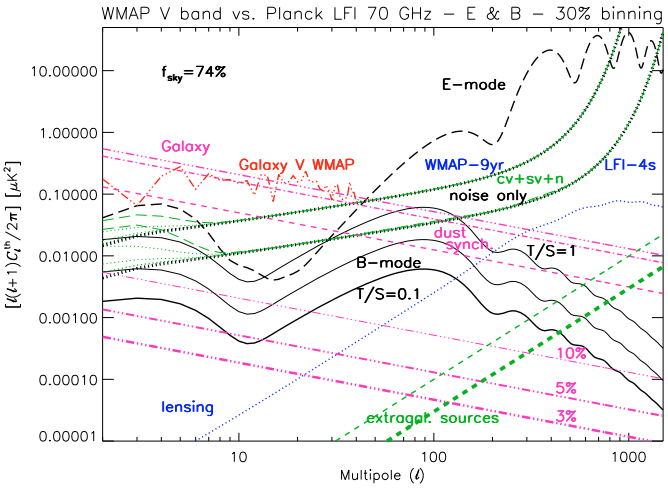

Fig. 4. As in Fig. 3 but for the sensitivity of WMAP in V band and LFI at 70 GHz, and including also the comparison with Galactic and extragalactic polarised foregrounds. Galactic synchrotron (purple dashes) and dust (purple dot-dashes) polarised emissions produce the overall Galactic foreground (purple three dot-dashes). WMAP 3-yr power-law fits for uncorrelated dust and synchrotron have been used. For comparison, WMAP 3-yr results derived directly from the foreground maps using the HEALPix package (Górski et al. 2005) are shown over a suitable multipole range: power-law fits provide (generous) upper limits to the power at low multipoles. Residual contamination levels by Galactic foregrounds (purple three dot-dashes) are shown for 10%, 5%, and 3% of the map level, at increasing thickness. The residual contribution of unsubtracted extragalactic sources, $C_\ell^{\rm res,PS}$, and the corresponding uncertainty, $\delta C_\ell^{\rm res,PS}$, are also plotted as thick and thin green dashes. These are computed assuming a relative uncertainty $\delta\Pi/\Pi = \delta S_{\rm lim}/S_{\rm lim} = 10\%$ in the knowledge of their degree of polarisation and the determination of the source detection threshold. We assumed the same sky coverage as in Fig. 3. Clearly, foreground contamination is lower at 70 GHz than at 30 GHz, but, since CMB maps will be produced from a component separation layer (see Sects. 2.3 and 6.3) we considered the same sky region.

to model more accurately the polarised synchrotron emission, which needs to be removed to greater than the few percent level to detect primordial B modes for $r \lesssim 0.1$ (Efstathiou & Gratton 2009).

2.1.2. Cosmological parameters

Given the improvement relative to WMAP C_ℓ achievable with the higher sensitivity and resolution of *Planck* (as discussed in the previous section for LFI), correspondingly superior determination of cosmological parameters is expected. Of course, the better sensitivity and angular resolution of HFI channels compared to WMAP and LFI ones will highly contribute to the improvement in cosmological parameters measured using *Planck*.

We present here the comparison between determinations of a suitable set of cosmological parameters using data from WMAP, *Planck*, and *Planck*-LFI alone.

In Fig. 5 we compare the forecasts for 1σ and 2σ contours for 4 cosmological parameters of the WMAP5 best-fit ΛCDM cosmological model: the baryon density; the cold dark matter (CDM) density; reionization, parametrized by the Thomson optical depth τ; and the slope of the initial power spectrum. These results show the expectation for the *Planck* LFI 70 GHz channel alone after 14 months of observations (red lines), the *Planck* combined 70 GHz, 100 GHz, and 143 GHz channels for the same integration time (blue lines), and the WMAP five year observations (black lines). We assumed that the 70 GHz channels and the 100 GHz and 143 GHz are the representative channels for LFI and HFI (we note that for HFI we have used angular resolution and sensitivities as given in Table 1.3 of the *Planck* scientific programme prepared by The Planck Collaboration 2006), for cosmological purposes, respectively, and we assumed a coverage of ~70% of the sky. Figure 5 shows that HFI 100 GHz and 143 GHz channels are crucial for obtaining the most accurate cosmological parameter determination.

While we have not explicitly considered the other channels of LFI (30 GHz and 44 GHz) and HFI (at frequencies ≥217 GHz) we note that they are essential for achieving the accurate separation of the CMB from astrophysical emissions, particularly for polarisation.

The improvement in cosmological parameter precision for LFI (2 surveys) compared to WMAP5 (Dunkley et al. 2009; Komatsu et al. 2009) is clear from Fig. 5. This is maximized for the dark matter abundance Ω_c because of the performance of the LFI 70 GHz channel with respect to WMAP5. From Fig. 5 it is clear that the expected improvement for *Planck* in cosmological parameter determination compared to that of WMAP5 can open a new phase in our understanding of cosmology.

2.1.3. Primordial non-Gaussianity

Simple cosmological models assume Gaussian statistics for the anisotropies. However, important information may come from mild deviations from Gaussianity (see e.g., Bartolo et al. 2004,

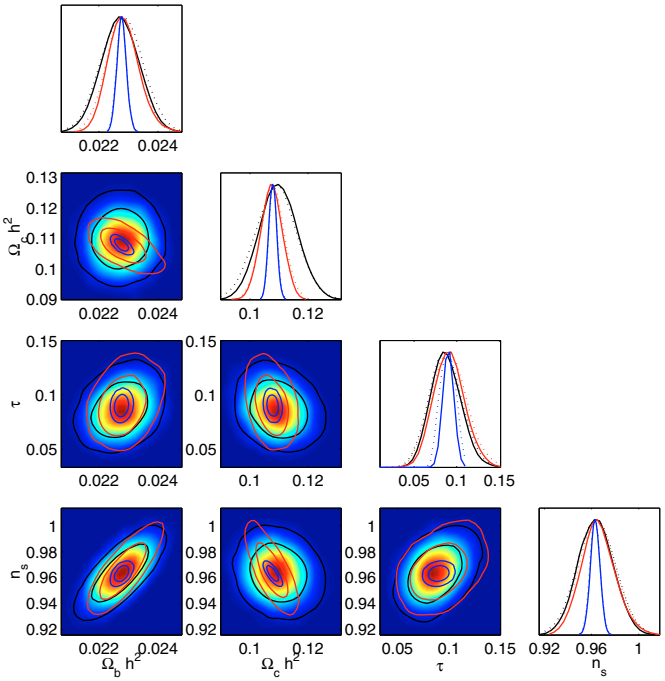

Fig. 5. Forecasts of 1σ and 2σ contours for the cosmological parameters of the WMAP5 best-fit ΛCDM cosmological model with reionization, as expected from *Planck* (blue lines) and from LFI alone (red lines) after 14 months of observations. The black contours are those obtained from WMAP five year observations. See the text for more details.

for a review). *Planck* total intensity and polarisation data will either provide the first true measurement of non-Gaussianity (NG) in the primordial curvature perturbations, or tighten the existing constraints (based on WMAP data, see footnote 3) by almost an order of magnitude.

Probing primordial NG is another activity that requires foreground cleaned maps. Hence, the full frequency maps of both instruments must be used for this purpose.

It is very important that the primordial NG is *model dependent*. As a consequence of the assumed flatness of the inflaton potential, any intrinsic NG generated during standard single-field slow-roll inflation is generally small, hence adiabatic perturbations originated by quantum fluctuations of the inflaton field during standard inflation are nearly Gaussian distributed. Despite the simplicity of the inflationary paradigm, however, the mechanism by which perturbations are generated has not yet been fully established and various alternatives to the standard scenario have been considered. Non-standard scenarios for the generation of primordial perturbations in single-field or multi-field inflation indeed permit higher NG levels. Alternative scenarios for the generation of the cosmological perturbations, such as the so-called curvaton, the inhomogeneous reheating, and DBI scenarios (Alishahiha et al. 2004), are characterized by a typically high NG level. For this reason, detecting or even just constraining primordial NG signals in the CMB is one of the most promising ways to shed light on the physics of the early Universe.

The standard way to parameterize primordial non-Gaussianity involves the parameter $f_{\rm NL}$, which is typically small. A positive detection of $f_{\rm NL} \sim 10$ would imply that all standard single-field slow-roll models of inflation are ruled out. In contrast, an improvement to the limits on the amplitude of $f_{\rm NL}$ will allow one to strongly reduce the class of non-standard inflationary models allowed by the data, thus providing unique insight into the fluctuation generation mechanism. At the same time, *Planck* temperature and polarisation data will allow different predictions of the *shape* of non-Gaussianities to be tested beyond the simple $f_{\rm NL}$ parameterization. For simple, quadratic non-Gaussianity of constant $f_{\rm NL}$, the angular bispectrum is dominated by "squeezed" triangle configurations with $\ell_1 \ll \ell_2, \ell_3$. This "local" NG is typical of models that produce the perturbations immediately after inflation (such as for the curvaton or the inhomogeneous reheating scenarios). So-called DBI inflation models, based on non-canonical kinetic terms for the *inflaton*, lead to non-local forms of NG, which are dominated by equilateral triangle configurations. It has been pointed out (Holman & Tolley 2008) that excited initial states of the inflaton may lead to a third shape, called "flattened" triangle configuration.

The strongest available CMB limits on $f_{\rm NL}$ for local NG comes from WMAP5. In particular, Smith et al. (2009) obtained $-4 < f_{\rm NL} < 80$ at 95% confidence level (C.L.) using the optimal estimator of local NG. *Planck* total intensity and polarisation data will allow the window on $|f_{\rm NL}|$ to be reduced below ∼10. Babich & Zaldarriaga (2004) and Yadav et al. (2007) demonstrated that a sensitivity to local non-Gaussianity $\Delta f_{\rm NL} \approx 4$ (at 1σ) is achievable with *Planck*. We note that accurate measurement of E-type polarisation will play a significant role in this constraint. Note also that the limits that *Planck* can achieve in this case are very close to those of an "ideal" experiment. Equilateral-shape NG is less strongly constrained at present, with $-125 < f_{\rm NL} < 435$ at 95% C.L. (Senatore et al. 2010). In this case, *Planck* will also have a strong impact on this constraint. Various authors (Bartolo & Riotto 2009) have estimated that *Planck* data will allow us to reduce the bound on $|f_{\rm NL}|$ to around 70.

Measuring the primordial non-Gaussianity in CMB data to these levels of precision requires accurate handling of possible contaminants, such as those introduced by instrumental noise and systematics, by the use of masks and imperfect foreground and point source removal.

2.1.4. Large-scale anomalies

Observations of CMB anisotropies contributed significantly to the development of the standard cosmological model, also known as the ΛCDM concordance model. This involves a set of basic quantities for which CMB observations and other cosmological and astrophysical data-sets agree: spatial curvature close to zero; ≃70% of the cosmic density in the form of dark energy; ≃20% in CDM; 4−5% in baryonic matter; and a nearly scale-invariant adiabatic, Gaussian primordial perturbations. Although the CMB anisotropy pattern obtained by WMAP is largely consistent with the concordance ΛCDM model, there are some interesting and curious deviations from it, in particular on the largest angular scales. Probing these deviations has required careful analysis procedures and so far are at only modest levels of significance. The anomalies can be listed as follows:

– Lack of power on large scales. The angular correlation function is found to be uncorrelated (i.e., consistent with zero) for angles larger than 60°. In Copi et al. (2007, 2009), it was shown that this event happens in only 0.03% of realizations of the concordance model. This is related to the surprisingly low amplitude of the quadrupole term of the angular power spectrum already found by COBE (Smoot et al. 1992; Hinshaw et al. 1996), and now confirmed by WMAP (Dunkley et al. 2009; Komatsu et al. 2009).

- Hemispherical asymmetries. It is found that the power coming separately from the two hemispheres (defined by the ecliptic plane) is quite asymmetric, especially at low ℓ (Eriksen et al. 2004a,b; Hansen et al. 2004).
- Unlikely alignments of low multipoles. An unlikely (for a statistically isotropic random field) alignment of the quadrupole and the octupole (Tegmark et al. 2003; Copi et al. 2004; Schwarz et al. 2004; Land & Magueijo 2005). Both quadrupole and octupole align with the CMB dipole (Copi et al. 2007). Other unlikely alignments are described in Abramo et al. (2006), Wiaux et al. (2006) and Vielva et al. (2007).
- Cold Spot. Vielva et al. (2004) detected a localized non-Gaussian behaviour in the southern hemisphere using a wavelet analysis technique (see also Cruz et al. 2005).

It is still unknown whether these anomalies are indicative of new (and fundamental) physics beyond the concordance model or whether they are simply the residuals of imperfectly removed astrophysical foreground or systematic effects. *Planck* data will provide a valuable contribution, not only in refining the cosmological parameters of the standard cosmological model but also in solving the aforementioned puzzles, because of the superior foreground removal and control of systematic effects, as well as *Planck*'s different scan strategy and wider frequency range compared with WMAP. In particular, the LFI 70 GHz channel will be crucial, since, as shown by WMAP, the foreground on large angular scales reaches a minimum in the *V* band.

2.2. Astrophysics

The accuracy of the extraction of the CMB anisotropy pattern from *Planck* maps largely relies, particularly for polarisation, on the quality of the separation of the *background* signal of cosmological origin from the various *foreground* sources of astrophysical origin that are superimposed on the maps (see also Sect. 2.3). The scientific case for *Planck* was presented by The Planck Collaboration (2006) and foresees the full exploitation of the multifrequency data. This is aimed not only at the extraction of the CMB, but also at the separation and study of each astrophysical component, using *Planck* data alone or in combination with other data-sets. This section provides an update of the scientific case, with particular emphasis on the contribution of the LFI to the science goals.

2.2.1. Galactic astrophysics

Planck will carry out an all-sky survey of the fluctuations in Galactic emission at its nine frequency bands. The HFI channels at $\nu \geq 100$ GHz will provide the main improvement with respect to COBE characterizing the large-scale Galactic dust emission[6], which is still poorly known, particularly in polarisation. However, since Galactic dust emission still dominates over free-free and synchrotron at 70 GHz (see e.g. Gold et al. 2009, and references therein), LFI will provide crucial information about the low frequency tail of this component. The LFI frequency channels, in particular those at 30 GHz and 44 GHz, will be relevant to the study of the diffuse, significantly polarised synchrotron emission and the almost unpolarised free-free emission.

[6] At far-IR frequencies significantly higher than those covered by *Planck*, much information comes from *IRAS* (see e.g., Miville-Deschênes & Lagache 2005, for a recent version of the maps).

Results from WMAP's lowest frequency channels inferred an additional contribution, probably correlated with dust (see Dobler et al. 2009, and references therein). While a model with complex synchrotron emission pattern and spectral index cannot be excluded, several interpretations of microwave (see e.g. Hildebrandt et al. 2007; Bonaldi et al. 2007) and radio (La Porta et al. 2008) data, and in particular the ARCADE 2 results (Kogut et al. 2009), seem to support the identification of this anomalous component as spinning dust (Draine & Lazarian 1998; Lazarian & Finkbeiner 2003). LFI data, at 30 GHz in particular, will shed new light on this intriguing question.

Another interesting component that will be studied by *Planck* data is the so-called "haze" emission in the inner Galactic region, possibly generated by synchrotron emission from relativistic electrons and positrons produced in the annihilations of dark matter particles (see e.g., Hooper et al. 2007; Cumberbatch et al. 2009; Hooper et al. 2008, and references therein).

Furthermore, the full interpretation of the Galactic diffuse emissions in *Planck* maps will benefit from a joint analysis with both radio and far-IR data. For instance, PILOT (Bernard et al. 2007) will improve on Archeops results (Ponthieu et al. 2005), measuring polarised dust emission at frequencies higher than 353 GHz, and BLAST-Pol (Marsden et al. 2008) at even higher frequencies. All-sky surveys at 1.4 GHz (see e.g., Burigana et al. 2006, and references therein) and in the range of a few GHz to 15 GHz will complement the low frequency side (see e.g., PGMS, Haverkorn et al. 2007; C-BASS, Pearson & C-BASS collaboration 2007; QUIJOTE, Rubino-Martin et al. 2008; and GEM, Barbosa et al. 2006) allowing an accurate multifrequency analysis of the depolarisation phenomena at low and intermediate Galactic latitudes. Detailed knowledge of the underlying noise properties in *Planck* maps will allow one to measure the correlation characteristics of the diffuse component, greatly improving physical models of the interstellar medium (ISM). The ultimate goal of these studies is the development of a consistent Galactic 3D model, which includes the various components of the ISM, and large and small scale magnetic fields (see e.g., Waelkens et al. 2009), and turbulence phenomena (Cho & Lazarian 2003).

While having moderate resolution and being limited in flux to a few hundred mJy, *Planck* will also provide multifrequency, all-sky information about discrete Galactic sources. This will include objects from the early stages of massive stars to the late stages of stellar evolution (Umana et al. 2006), from HII regions to dust clouds (Pelkonen et al. 2007). Models for both the enrichment of the ISM and the interplay between stellar formation and ambient physical properties will be also tested.

Planck will also have a chance to observe some Galactic micro-blazars (such as e.g., Cygnus X-3) in a flare phase and perform multifrequency monitoring of these events on timescales from hours to weeks. A quick detection software (QDS) system was developed by a Finnish group in collaboration with LFI DPC (Aatrokoski et al. 2010). This will be used to identify of source flux variation, in *Planck* time ordered data.

Finally, *Planck* will provide unique information for modelling the emission from moving objects and diffuse interplanetary dust in the Solar System. The mm and sub-mm emission from planets and up to 100 asteroids will also be studied (Cremonese et al. 2002; Maris & Burigana 2009). The zodiacal light emission will also be measured to great accuracy, free from residual Galactic contamination (Maris et al. 2006b).

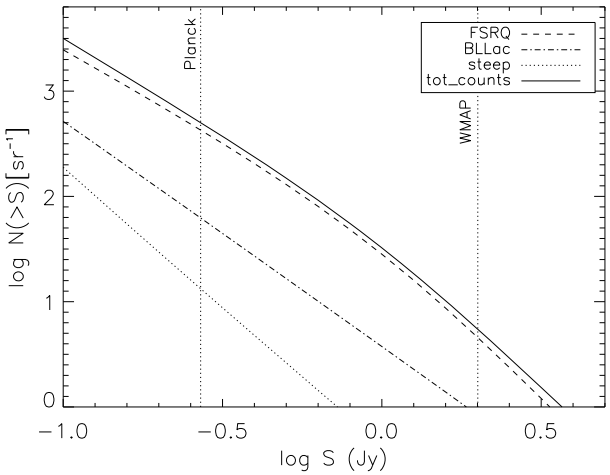

Fig. 6. Integral counts of different radio source populations at 70 GHz, predicted by the de Zotti et al. (2005) model: flat-spectrum radio quasars; BL Lac objects; and steep-spectrum sources. The vertical dotted lines show the estimated completeness limits for *Planck* and WMAP (61 GHz) surveys.

2.2.2. Extragalactic astrophysics

The higher sensitivity and angular resolution of LFI compared to WMAP will allow us to obtain substantially richer samples of extragalactic sources at mm wavelengths. Applying a new multi-frequency linear filtering technique to realistic LFI simulations of the sky, Herranz et al. (2009) detected 1600, 1550, and 1000 sources with 95% reliability at 30, 44, and 70 GHz, respectively, over about 85% of the sky. The 95% completeness fluxes are 540, 340, and 270 mJy at 30, 44, and 70 GHz, respectively. For comparison, the total number of $|b| > 5°$ sources detected by Massardi et al. (2009) at $\geq 5\sigma$ in WMAP5 maps at 33, 41, and 61 GHz (including several possibly spurious objects), are 307, 301, and 161, respectively; the corresponding detection limits increase from $\simeq$1 Jy at 23 GHz, to $\simeq$2 Jy at 61 GHz. The number of detections reported by Wright et al. (2009) is lower by about 20%.

As illustrated in Fig. 6, the far larger source sample expected from *Planck* will allow us to obtain good statistics for different subpopulations of sources, some of which are not (or only poorly) represented in the WMAP sample. The dominant radio population at LFI frequencies consists of flat-spectrum radio quasars, for which LFI will provide a bright sample of $\geq$1000 objects, well suited to cover the parameter space of current physical models. Interestingly, the expected numbers of blazars and BL Lac objects detectable by LFI are similar to those expected from the Fermi Gamma-ray Space Telescope (formerly GLAST; Abdo 2009; Atwood et al. 2009). It is likely that the LFI and the Fermi blazar samples will have a substantial overlap, making it possible to more carefully define the relationships between radio and gamma-ray properties of these sources than has been possible so far. The analysis of spectral properties of the ATCA 20 GHz bright sample indicates that quite a few high-frequency selected sources have peaked spectra; most of them are likely to be relatively old, beamed objects (blazars), whose radio emission is dominated by a single knot in the jet caught in a flaring phase. The *Planck* sample will allow us to obtain key information about the incidence and timescales of these flaring episodes, the distribution of their peak frequencies, and therefore the propagation of the flare along the jet. A small fraction of sources exhibiting high frequency peaks may be extreme high frequency peakers (Dallacasa et al. 2000), understood to be newly born radio sources (ages as low as thousand years). Obviously, the discovery of just a few of these sources would be extremely important for sheding light on the poorly understood mechanisms that trigger the radio activity of Galactic cores.

WMAP has detected polarised fluxes at $\geq 4\sigma$ in two or more bands for only five extragalactic sources (Wright et al. 2009). LFI will substantially improve on this, providing polarisation measurements for tens of sources, thus allowing us to obtain the first statistically meaningful unbiased sample for polarisation studies at mm wavelengths. It should be noted that *Planck* polarisation measurements will not be confusion-limited, as in the case of total flux, but noise-limited. Thus the detection limit for polarised flux in *Planck*-LFI channels will be $\simeq$200−300 mJy, i.e., lower than for the total flux.

As mentioned above, the astrophysics programme of *Planck* is much wider than that achievable with LFI alone, both because the specific role of HFI and, in particular, the great scientific synergy between the two instruments. One noteworthy example is the *Planck* contribution to the astrophysics of clusters. *Planck* will detect $\approx 10^3$ galaxy clusters out to redshifts of order unity by means of their thermal Sunyaev-Zel'dovich effect (Leach et al. 2008; Bartlett et al. 2008). This sample will be extremely important for understanding both the formation of large-scale structure and the physics of the intracluster medium. To perform these measurements, a broad spectral coverage, i.e., the combination of data from both *Planck* instruments (LFI and HFI), is a key asset. This combination, supplemented by ground-based, follow-up observations planned by the *Planck* team, will allow, in particular, accurate correction for the contamination by radio sources (mostly due to the high quality of the LFI channels) and dusty galaxies (HFI channels), either associated with the clusters or in their foreground/background (Lin et al. 2009).

2.3. Scientific data analysis

The data analysis process for a high precision experiment such as LFI must be capable of reducing the data volume by several orders of magnitude with minimal loss of information. The sheering size of the data set, the high sensitivity required to achieve the science goals, and the significance of the statistical and systematic sources of error all conspire to make data analysis a far from trivial task.

The map-making layer provides a lossless compression by several orders of magnitude, projecting the data set from the time domain to the discretized celestial sphere (Janssen & Gulkis 1992; Lineweaver et al. 1994; Wright et al. 1996; Tegmark 1997). Furthermore, timeline-specific instrumental effects that are not scan-synchronous are reduced in magnitude when projected from time to pixel space (see e.g., Mennella et al. 2002) and, in general, the analysis of maps provides a more convenient means of assessing the level of systematics compared to timeline analysis.

Several map-making algorithms have been proposed to produce sky maps in total intensity (Stokes I) and linear polarisation (Stokes Q and U) from the LFI timelines. So-called "destriping" algorithms have historically first been applied. These take advantage of the details of the *Planck* scanning strategy to suppress correlated noise (Maino et al. 1999). Although computationally efficient, these methods do not, in general, yield a minimum variance map. To overcome this problem, minimum-variance map-making algorithms have been devised and implemented specifically for LFI (Natoli et al. 2001; de Gasperis et al. 2005).

The latter are also known as generalized least squares (GLS) methods and are accurate and flexible. Their drawback is that, at the size of the *Planck* data set, they require a significant amount of massively powered computational resources (Poutanen et al. 2006; Ashdown et al. 2007, 2009) and are thus infeasible to use within a Monte Carlo context. To overcome the limitations of GLS algorithms, the LFI community has developed so-called "hybrid" algorithms (Keihänen et al. 2005; Kurki-Suonio et al. 2009; Keihänen et al. 2010). These algorithms rely on a tunable parameter connected to the $1/f$ knee frequency, a measure of the amount of low frequency correlated noise in the time-ordered data: the higher the knee frequency, the shorter the "baseline" length needed to be chosen to properly suppress the $1/f$ contribution. From this point of view, the GLS solution can be thought of as the limiting case when the baseline length approaches the sampling interval. Provided that the knee frequency is not too high, hybrid algorithms can achieve GLS accuracy at a fraction of the computational demand. Furthermore, they can be tuned to the desired precision when speed is an issue (e.g., for timeline-to-map Monte Carlo production). The baseline map-making algorithms for LFI is a hybrid code dubbed MADAM.

Map-making algorithms can, in general, compute the correlation (inverse covariance) matrix of the map estimate that they produce (Keskitalo et al. 2010). At high resolution this computation, though feasible, is impractical, because the size of the matrix makes its handling and inversion prohibitively difficult. At low resolution, the covariance matrix will be produced instead: this is of extreme importance for the accurate characterization of the low multipoles of the CMB (Keskitalo et al. 2010; Gruppuso et al. 2009).

A key tier of *Planck* data analysis is the separation of astrophysical from cosmological components. A variety of methods have been developed to this end (e.g., Leach et al. 2008). Point source extraction is achieved by exploiting non-*Planck* catalogues, as well as filtering *Planck* maps with optimal functions (wavelets) capable of recognizing beam-like patterns. In addition to linearly combining the maps or fitting for known templates, diffuse emissions are separated by using the statistical distributions of the different components, assuming independence between them, or by means of a suitable parametrization and fitting of foreground unknowns on the basis of spatial correlations in the data or, in alternative, multi-frequency single resolution elements only.

The extraction of statistical information from the CMB usually proceeds by means of correlation functions. Since the CMB field is Gaussian to a large extent (e.g. Smith et al. 2009), most of the information is encoded in the two-point function or equivalently in its reciprocal representation in spherical harmonics space. Assuming rotational invariance, the latter quantity is well described by the set of C_ℓ (see e.g., Gorski 1994). For an ideal experiment, the estimated power spectrum could be directly compared to a Boltzmann code prediction to constrain the cosmological parameters. However, in the case of incomplete sky coverage (which induces couplings among multipoles) and the presence of noise (which, in general, is not rotationally invariant because of the coupling between correlated noise and scanning strategy), a more thorough analysis is necessary. The likelihood function for a Gaussian CMB sky can be easily written and provides a sound mechanism for constraining models and data. The direct evaluation of this function, however, poses intractable computational issues. Fortunately, only the lowest multipoles require exact treatment. This can be achieved either by direct evaluation in the pixel domain or sampling the posterior distribution of the CMB using sampling methods such as the Gibbs approach (Jewell et al. 2004; Wandelt et al. 2004). At high multipoles, where the likelihood function cannot be evaluated exactly, a wide range of effective, computationally affordable approximations exist (see e.g., Hamimeche & Lewis 2008; and Rocha et al., in prep., and references therein). The low and high ℓ approaches to power spectrum estimation will be joined into a hybrid procedure, pioneered by Efstathiou (2004).

The data analysis of LFI will require daunting computational resources. In view of the size and complexity of its data set, accurate characterization of the scientific results and error propagation will be achieved by means of a massive use of Monte Carlo simulations. A number of worldwide distributed supercomputer centres will support the DPC in this activity. A partial list includes NERSC-LBNL in the USA, CINECA in Italy, CSC in Finland, and MARE NOSTRUM in Spain. The European centres will benefit from the Distributed European Infrastructure for Supercomputer Application[7].

3. Instrument

3.1. Optics

During the design phase of LFI, great effort was dedicated to the optical design of the focal plane unit (FPU). As already mentioned in the introduction, the actual design of the *Planck* telescope is derived from COBRAS and specially has been tuned by subsequent studies of the LFI team (Villa et al. 1998) and Thales-Alenia Space. These studies demonstrated the importance of increasing the telescope diameter (Mandolesi et al. 2000), optimizing the optical design, and also showed how complex it would be to match the real focal surface to the horn phase centres (Valenziano et al. 1998). The optical design of LFI is the result of a long iteration process in which the optimization of the position and orientation of each feed horn involves a trade-off between angular resolution and sidelobe rejection levels (Sandri et al. 2004; Burigana et al. 2004; Sandri et al. 2010). Tight limits were also imposed by means of mechanical constraints. The 70 GHz system has been improved in terms of the single horn design and its relative location in the focal surface. As a result, the angular resolution has been maximized.

The feed horn development programme started in the early stages of the mission with prototype demonstrators (Bersanelli et al. 1998), followed by the elegant bread board (Villa et al. 2002) and finally by the qualification (D'Arcangelo et al. 2005) and flight models (Villa et al. 2009). The horn design has a corrugated shape with a dual profile (Gentili et al. 2000). This choice was justified by the complexity of the optical interfaces (coupling with the telescope and focal plane horn accommodation) and the need to respect the interfaces with HFI.

Each of the corrugated horns feeds an orthomode transducer (OMT) that splits the incoming signal into two orthogonal polarised components (D'Arcangelo et al. 2009a). The polarisation capabilities of the LFI are guaranteed by the use of OMTs placed immediately after the corrugated horns. While the incoming polarisation state is preserved inside the horn, the OMT divides it into two linear orthogonal polarisations, allowing LFI to measure the linear polarisation component of the incoming sky signal. The typical value of OMT cross-polarisation is about −30 dB, setting the spurious polarisation of the LFI optical interfaces at a level of 0.001.

[7] http://www.deisa.eu

Table 2. LFI optical performance.

	ET	*FWHM*	*e*	XPD	Ssp	Msp
70	17 dB at 22°	13.03	1.22	−34.73	0.17	0.65
44	30 dB at 22°	26.81	1.26	−30.54	0.074	0.18
30	30 dB at 22°	33.34	1.38	−32.37	0.24	0.59

Notes. All the values are averaged over all channels at the same frequency. ET is the horn edge taper measured at 22° from the horn axis; *FWHM* is the angular resolution in arcmin; *e* is the ellipticity; XPD is the cross-polar discrimination in dB; Ssp is the Sub-reflector spillover (%); Msp is the Main-reflector spillover (%). See text for details.

Table 2 shows the overall LFI optical characteristics expected in-flight (Tauber et al. 2010). The edge taper (ET) values, quoted in Table 2, refer to the horn taper; they are reference values assumed during the design phase and do not correspond to the true edge taper on the mirrors (see Sandri et al. 2010, for details). The reported angular resolution is the average *FWHM* of all the channels at the same frequency. The cross-polar discrimination (XPD) is the ratio of the antenna solid angle of the cross-polar pattern to the antenna solid angle of the co-polar pattern, both calculated within the solid angle of the −3 dB contour. The main- and sub-reflector spillovers represent the fraction of power that reach the horns without being intercepted by the main- and sub-reflectors, respectively.

3.2. Radiometers

LFI is designed to cover the low frequency portion of the wide-band *Planck* all-sky survey. A detailed description of the design and implementation of the LFI instrument is given in Bersanelli et al. (2010) and references therein, while the results of the on-ground calibration and test campaign are presented in Mennella et al. (2010) and Villa et al. (2010). The LFI is an array of cryogenically cooled radiometers designed to observe in three frequency bands centered on 30 GHz, 44 GHz, and 70 GHz with high sensitivity and practically no systematic errors. All channels are sensitive to the I, Q, and U Stokes parameters, thus providing information about both temperature and polarisation anisotropies. The heart of the LFI instrument is a compact, 22-channel multifrequency array of differential receivers with cryogenic low-noise amplifiers based on indium phosphide (InP) HEMTs. To minimise the power dissipation in the focal plane unit, which is cooled to 20 K, the radiometers are divided into two subassemblies (the front-end module, FEM, and the back-end module, BEM) connected by a set of composite waveguides, as shown in Fig. 7. Miniaturized, low-loss passive components are implemented in the front end for optimal performance and compatibility with the stringent thermo-mechanical requirements of the interface with the HFI.

The radiometer was designed to suppress $1/f$-type noise induced by gain and noise temperature fluctuations in the amplifiers, which would otherwise be unacceptably high for a simple, total-power system. A differential pseudo-correlation scheme is adopted, in which signals from the sky and from a black-body reference load are combined by a hybrid coupler, amplified by two independent amplifier chains, and separated by a second hybrid (Fig. 8). The sky and the reference load power can then be measured and their difference calculated. Since the reference signal has been affected by the same gain variations in the two amplifier chains as the sky signal, the sky power can be recovered to high precision. Insensitivity to fluctuations in the back-end amplifiers and detectors is realized by switching phase shifters at 8 kHz synchronously in each amplifier chain. The rejection of $1/f$ noise as well as immunity to other systematic effects is optimised if the two input signals are nearly equal. For this reason, the reference loads are cooled to 4 K (Valenziano et al. 2009) by mounting them on the 4 K structure of the HFI. In addition, the effect of the residual offset (<1 K in nominal conditions) is reduced by introducing a gain modulation factor in the onboard processing to balance the output signal. As shown in Fig. 8, the differencing receiver greatly improves the stability of the measured signal (see also Fig. 8 in Bersanelli et al. 2010).

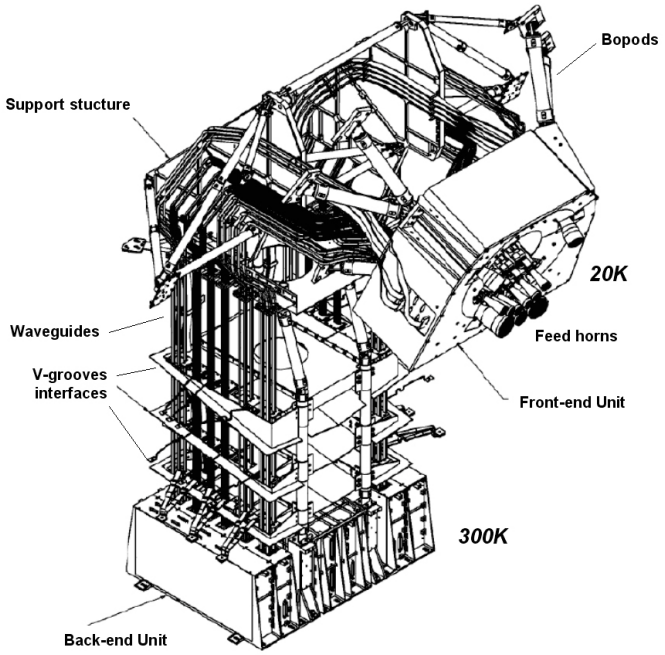

Fig. 7. The LFI radiometer array assembly, with details of the front-end and back-end units. The front-end radiometers are based on wide-band low-noise amplifiers, fed by corrugated feedhorns which collect the radiation from the telescope. A set of composite waveguides transport the amplified signals from the front-end unit (at 20 K) to the back-end unit (at 300 K). The waveguides are designed to meet simultaneously radiometric, thermal, and mechanical requirements, and are thermally linked to the three V-Groove thermal shields of the *Planck* payload module. The back-end unit, located on top of the *Planck* service module, contains additional amplification as well as the detectors, and is interfaced to the data acquisition electronics. The HFI is inserted into and attached to the frame of the LFI focal-plane unit.

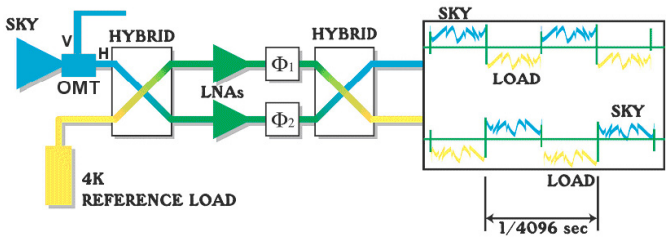

Fig. 8. Schematic of the LFI front-end radiometer. The front-end unit is located at the focus of the *Planck* telescope, and comprises: dual-profiled corrugated feed horns; low-loss (0.2 dB), wideband (>20%) orthomode transducers; and radiometer front-end modules with hybrids, cryogenic low noise amplifiers, and phase switches. For details see Bersanelli et al. (2010).

The LFI amplifiers at 30 GHz and 44 GHz use discrete InP HEMTs incorporated into a microwave integrated circuit (MIC). At these frequencies, the parasitics and uncertainties introduced by the bond wires in a MIC amplifier are controllable and the additional tuning flexibility facilitates optimization for low noise. At 70 GHz, there are twelve detector chains. Amplifiers at these frequencies use monolithic microwave integrated circuits (MMICs), which incorporate all circuit elements and the HEMT transistors on a single InP chip. At these frequencies, MMIC technology provides not only significantly superior performance to MIC technology, but also allows faster assembly and smaller sample-to-sample variance. Given the large number of amplifiers required at 70 GHz, MMIC technology can rightfully be regarded as an important development for the LFI.

Fourty-four waveguides connect the LFI front-end unit, cooled to 20 K by a hydrogen sorption cooler, to the back-end unit (BEU), which is mounted on the top panel of the *Planck* service module (SVM) and maintained at a temperature of 300 K. The BEU comprises the eleven BEMs and the data acquisition electronics (DAE) unit, which provides adjustable bias to the amplifiers and phase switches as well as scientific signal conditioning. In the back-end modules, the RF signals are amplified further in the two legs of the radiometers by room temperature amplifiers. The signals are then filtered and detected by square-law detector diodes. A DC amplifier then boosts the signal output, which is connected to the data acquisition electronics. After onboard processing, provided by the radiometer box electronics assembly (REBA), the compressed signals are down-linked to the ground station together with housekeeping data. The sky and reference load DC signals are transmitted to the ground as two separated streams of data to ensure optimal calculation of the gain modulation factor for minimal $1/f$ noise and systematic effects. The complexity of the LFI system called for a highly modular plan of testing and integration. Performance verification was first carried out at the single unit-level, followed by campaigns at sub-assembly and instrument level, then completed with full functional tests after integration into the *Planck* satellite. Scientific calibration has been carried out in two main campaigns, first on the individual radiometer chain assemblies (RCAs), i.e., the units comprising a feed horn and the two pseudo-correlation radiometers connected to each arm of the orthomode transducer (see Fig. 8), and then at instrument level. For the RCA campaign, we used sky loads and reference loads cooled close to 4 K which allowed us to perform an accurate verification of the instrument performance in near-flight conditions. Instrument level tests were carried out with loads at 20 K, which allowed us to verify the radiometer performance in the integrated configuration. Testing at the RCA and instrument level, both for the qualification model (QM) and the flight model (FM), were carried out at Thales Alenia Space, Vimodrone (Milano, Italy). Finally, system-level tests of the LFI integrated with HFI in the *Planck* satellite were carried out at Centre Spatial de Liège (CSL) in the summer of 2008.

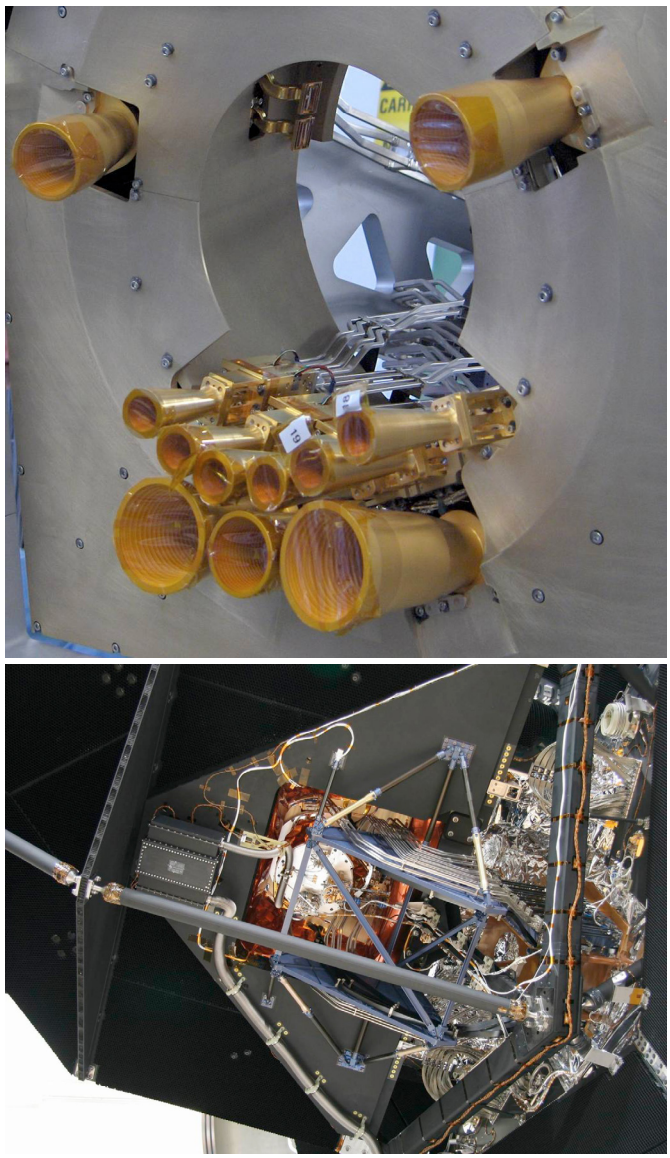

Fig. 9. *Top panel*: picture of the LFI focal plane showing the feed-horns and main frame. The central portion of the main frame is designed to provide the interface to the HFI front-end unit, where the reference loads for the LFI radiometers are located and cooled to 4 K. *Bottom panel*: a back-view of the LFI integrated on the *Planck* satellite. Visible are the upper sections of the waveguides interfacing the front-end unit, as well as the mechanical support structure.

3.3. Sorption cooler

The SCS is the first active element of the *Planck* cryochain. Its purpose is to cool the LFI radiometers to their operational temperature of around 20 K, while providing a pre-cooling stage for the HFI cooling system, a 4.5 K mechanical Joule-Thomson cooler and a Benoit-style open-cycle dilution refrigerator. Two identical sorption coolers have been fabricated and assembled by the Jet Propulsion Laboratory (JPL) under contract to NASA. JPL has been a pioneer in the development and application of these cryo-coolers for space and the two *Planck* units are the first continuous closed-cycle hydrogen sorption coolers to be used for a space mission (Morgante et al. 2009).

Sorption refrigerators are attractive systems for cooling instruments, detectors, and telescopes when a vibration-free system is required. Since pressurization and evacuation is accomplished by simply heating and cooling the sorbent elements sequentially, with no moving parts, they tend to be very robust and generate essentially no vibrations on the spacecraft. This provides excellent reliability and a long life. By cooling using Joule-Thomson (J-T) expansion through orifices, the cold end can also be located remotely (thermally and spatially) from the warm end. This allows excellent flexibility in integrating the cooler with the cold payload and the warm spacecraft.

3.3.1. Specifications

The main requirements of the *Planck* SCS are summarized below:

- provision of about 1 W total heat lift at instrument interfaces using a ≤60 K pre-cooling temperature at the coldest V-groove radiator on the *Planck* spacecraft;
- maintain the following instrument interface temperatures:
  LFI at ≤22.5 K [80% of total heat lift],
  HFI at ≤19.02 K [20% of total heat lift];
- temperature stability (over one full cooler cycle ≈6000 s):
  ≤450 mK, peak-to-peak at HFI interface,
  ≤100 mK, peak-to-peak at LFI interface;
- input power consumption ≤470 W (at end of life, excluding electronics);
- operational lifetime ≥2 years (including testing).

3.3.2. Operations

The SCS consists of a thermo-mechanical unit (TMU, see Fig. 10) and electronics to operate the system. Cooling is produced by J-T expansion with hydrogen as the working fluid. The key element of the 20 K sorption cooler is the compressor, an absorption machine that pumps hydrogen gas by thermally cycling six compressor elements (sorbent beds). The principle of operation of the sorption compressor is based on the properties of a unique sorption material (a La, Ni, and Sn alloy), which can absorb a large amount of hydrogen at relatively low pressure, and desorb it to produce high-pressure gas when heated within a limited volume. Electrical resistances heat the sorbent, while cooling is achieved by thermally connecting, by means of gas-gap thermal switches, the compressor element to a warm radiator at 270 K on the satellite SVM. Each sorbent bed is connected to both the high-pressure and low-pressure sides of the plumbing system by check valves, which allow gas flow in a single direction only. To dampen oscillations on the high-pressure side of the compressor, a high-pressure stabilization tank (HPST) system is utilized. On the low-pressure side, a low-pressure storage bed (LPSB) filled with hydride, primarily operates as a storage bed for a large fraction of the H_2 inventory required to operate the cooler during flight and ground testing while minimizing the pressure in the non-operational cooler during launch and transportation. The compressor assembly mounts directly onto the warm radiator (WR) on the spacecraft. Since each sorbent bed is taken through four steps (heat up, desorption, cool-down, absorption) in a cycle, it will intake low-pressure hydrogen and output high-pressure hydrogen on an intermittent basis. To produce a continuous stream of liquid refrigerant, the sorption beds phases are staggered so that at any given time, one is desorbing while the others are heating up, cooling down, or re-absorbing low-pressure gas.

The compressed refrigerant then travels in the piping and cold-end assembly (PACE, see Fig. 10), through a series of heat exchangers linked to three V-Groove radiators on the spacecraft that provide passive cooling to approximately 50 K. Once pre-cooled to the required range of temperatures, the gas is expanded through the J-T valve. Upon expansion, hydrogen forms liquid droplets whose evaporation provides the cooling power. The liquid/vapour mixture then sequentially flows through the two Liquid Vapour Heat eXchangers (LVHXs) inside the cold end. LVHX1 and 2 are thermally and mechanically linked to the corresponding instrument (HFI and LFI) interface. The LFI is coupled to LVHX2 through an intermediate thermal stage, the temperature stabilization assembly (TSA). A feedback control loop

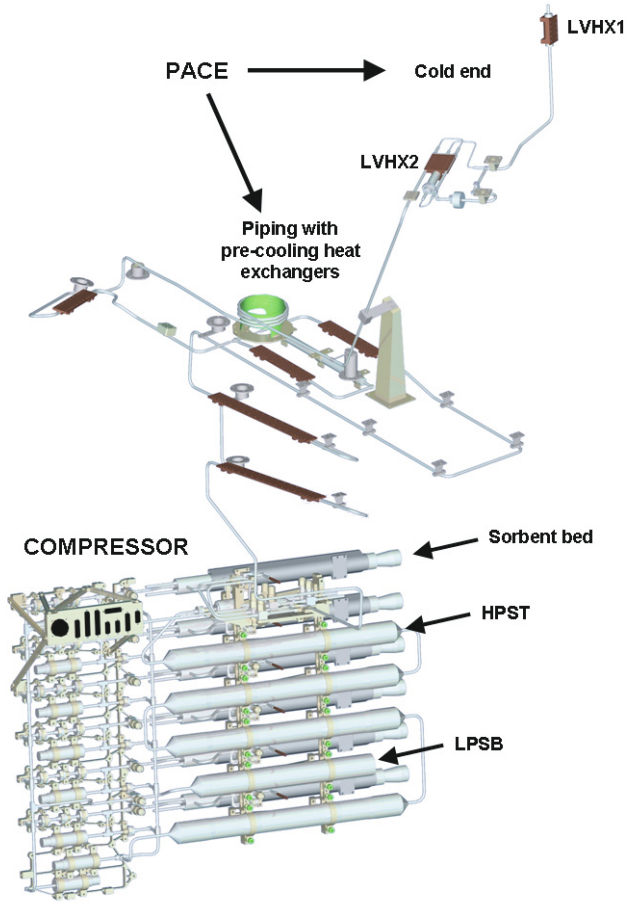

Fig. 10. SCS thermo-mechanical unit. See Appendix A for acronyms.

(PID type), operated by the cooler electronics, is able to control the TSA peak-to-peak fluctuations down to the required level (≤100 mK). Heat from the instruments evaporates liquid hydrogen and the low pressure gaseous hydrogen is circulated back to the cold sorbent beds for compression.

3.3.3. Performance

The two flight sorption cooler units were delivered to ESA in 2005. Prior to delivery, in early 2004, both flight models underwent subsystem-level thermal-vacuum test campaigns at JPL. In spring 2006 and summer 2008, respectively, SCS redundant and nominal units were tested in cryogenic conditions on the spacecraft FM at the CSL facilities. The results of these two major test campaigns are summarized in Table 3 and reported in full detail in Morgante et al. (2009).

4. LFI programme

The model philosophy adopted for LFI and the SCS was chosen to meet the requirements of the ESA *Planck* system which assumed from the beginning that there would be three development models of the satellite:

- The *Planck* avionics model (AVM) in which the system bus was shared with the *Herschel* satellite, and allowed basic electrical interface testing of all units and communications protocol and software interface verification.
- The *Planck* qualification model (QM), which was limited to the *Planck* payload module (PPLM) containing QMs of LFI,

Table 3. SCS flight units performance summary.

SCS Unit	Warm Rad. T(K)	3 rd VGroove T(K)	Cold-end T(K) HFI I/F	Cold-end T(K) LFI I/F	Heat lift (mW)	Input power (V)	Cycle time (s)
	270.5	45	17.2	18.7[a,b]	1100	297	940
Redundant	277	60	18.0	20.1[a,b]	1100	460	492
	282.6	60	18.4	19.9[a,b]	1050	388	667
Nominal	270	47	17.1	18.7[a]	1125	304	940
	273	48	17.5	18.7[a]	N/A[c]	470	525

Notes. [(a)] Measured at temperature stabilization assembly (TSA) stage; [(b)] in SCS-redundant test campaign TSA stage active control was not enabled; [(c)] not measured.

HFI, and the *Planck* telescope and structure that would allow a qualification vibration test campaign to be performed at payload level, as well as alignment checks, and would, in particular, allow a cryogenic qualification test campaign to be performed on all the advanced instrumentation of the payload that had to fully perform in cryogenic conditions.

– The *Planck* protoflight model (PFM) which contained all the flight model (FM) hardware and software that would undergo the PFM environmental test campaign, culminating in extended thermal and cryogenic functional performance tests.

4.1. Model philosophy

In correspondence with the system model philosophy, it was decided by the *Planck* consortium to follow a conservative incremental approach involving prototype demonstrators.

4.1.1. Prototype demonstrators (PDs)

The scope of the PDs was to validate the LFI radiometer design concept giving early results on intrinsic noise, particularly $1/f$ noise properties, and characterise systematic effects in a preliminary fashion to provide requirement inputs to the remainder of the instrument design and at satellite level. The PDs also have the advantage of being able to test and gain experience with very low noise HEMT amplifiers, hybrid couplers, and phase switches. The PD development started early in the programme during the ESA development pre-phase B activity and ran in parallel with the successive instrument development phase of elegant breadboarding.

4.1.2. Elegant breadboarding (EBB)

The purpose of the LFI EBBs was to demonstrate the maturity of the full radiometer design across the whole frequency range of LFI prior to initiating qualification model construction. Thus, full comparison radiometers (two channels covering a single polarisation direction) were constructed, centred on 100 GHz, 70 GHz, and 30 GHz, extending from the expected design of the corrugated feed-horns at their entrance to their output stages at their back-end. These were put through functional and performance tests with their front-end sections operating at 20 K as expected in-flight. It was towards the end of this development that the financial difficulties that terminated the LFI 100 GHz channel development hit the programme.

4.1.3. The qualification model (QM)

The development of the LFI QM commenced in parallel with the EBB activities. From the very beginning, it was decided that only a limited number of radiometer chain assemblies (RCA), each containing four radiometers (and thus fully covering two orthogonal polarisation directions) at each frequency should be included and that the remaining instrumentation would be represented by thermal mechanical dummies. Thus, the LFI QM contained 2 RCA at 70 GHz and one each at 44 GHz and 30 GHz. The active components of the data acquisition electronics (DAE) were thus dimensioned accordingly. The radiometer electronics box assembly (REBA) QM supplied was a full unit. All units and assemblies went through approved unit level qualification level testing prior to integration as the LFI QM in the facilities of the instrument prime contractor Thales Alenia Space Milano.

The financial difficulties also disrupted the QM development and led to the use by ESA of a thermal-mechanical representative dummy of LFI in the system level satellite QM test campaign because of the ensuing delay in the availability of the LFI QM. The LFI QM was however fundamental to the development of LFI as it enabled the LFI consortium to perform representative cryotesting of a reduced model of the instrument and thus confirm the design of the LFI flight model.

4.1.4. The flight model (FM)

The LFI FM contained flight standard units and assemblies that went through flight unit acceptance level tests prior to integration in to the LFI FM. In addition, prior to mounting in the LFI FM, each RCA went through a separate cryogenic test campaign after assembly to allow preliminary tuning and confirm the overall functional performance of each radiometer. At the LFI FM test level the instrument went through an extended cryogenic test campaign that included further tuning and instrument calibration that could not be performed when mounted in the final configuration on the satellite because of schedule and cost constraints. At the time of delivery of the LFI FM to ESA for integration on the satellite, the only significant verification test that remained to be done was the vibration testing of the fully assembled radiometer array assembly (RAA). This could not be performed in a meaningful way at instrument level because of the problem of simulating the coupled vibration input through the DAE and the LFI FPU mounting to the RAA (and in particular into the waveguides). Its verification was completed successfully during the satellite PFM vibration test campaign.

4.1.5. The avionics model (AVM)

The LFI AVM was composed of the DAE QM, and its secondary power supply box removed from the RAA of the LFI QM, an AVM model of the REBA and the QM instrument harness. No radiometers were present in the LFI AVM, and their active inputs on the DAE were terminated with resistors. The LFI AVM

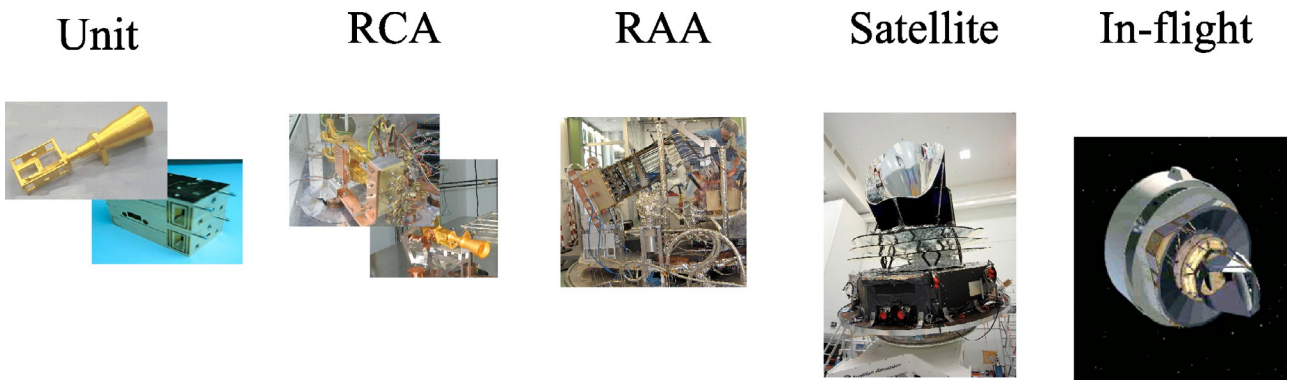

Fig. 11. Schematic of the various calibration steps in the LFI development.

was used successfully by ESA in the *Planck* System AVM test campaigns to fulfill its scope outlined above.

4.2. The sorption cooler subsystem (SCS) model philosophy

The SCS model development was designed to produce two coolers: a nominal cooler and a redundant cooler. The early part of the model philosophy adopted was similar to that of LFI, employing prototype development and the testing of key components, such as single compressor beds, prior to the building of an EBB containing a complete complement of components such as in a cooler intended to fly. This EBB cooler was submitted to an intensive functional and performance test campaign. The sorption cooler electronics (SCE) meanwhile started development with an EBB and was followed by a QM and then FM1/FM2 build.

The TMUs of both the nominal and redundant sorption coolers went through protoflight unit testing prior to assembly with their respective PACE for thermal/cryogenic testing before delivery. To conclude the qualification of the PACE, a spare unit participated in the PPLM QM system level vibration and cryogenic test campaign.

An important constraint in the ground operation of the sorption coolers is that they could not be fully operated with their compressor beds far from a horizontal position. This was to avoid permanent non-homogeneity in the distribution of the hydrides in the compressor beds and the ensuing loss in efficiency. In the fully integrated configuration of the satellite (the PFM thermal and cryogenic test campaign) for test chamber configuration, schedule and cost reasons would allow only one cooler to be in a fully operable orientation. Thus, the first cooler to be supplied, which was designated the redundant cooler (FM1), was mounted with the PPLM QM and put through a cryogenic test campaign (termed PFM1) with similar characteristics to those of the final thermal balance and cryogenic tests of the fully integrated satellite. The FM1 was then later integrated into the satellite where only short, fully powered, health checking was performed. The second cooler was designated as the nominal cooler (FM2) and participated fully in the final cryotesting of the satellite. For both coolers, final verification (TMU assembled with PACE) was achieved during the *Planck* system-level vibration-test campaign and subsequent tests.

The AVM of the SCS was supplied using the QM of the SCE and a simulator of the TMU to simulate the power load of a real cooler.

4.3. System level integration and test

The *Planck* satellite and its instruments, were integrated at the Thales Alenia Space facilities at Cannes in France. The SCS nominal and redundant coolers were integrated onto the *Planck* satellite before LFI and HFI.

Prior to integration on the satellite, the HFI FPU was integrated into the FPU of LFI. This involved mounting the LFI 4 K loads onto HFI before starting the main integration process, which was a very delicate operation considering that when performed the closest approach of LFI and HFI would be of the order of 2 mm. It should be remembered that LFI and HFI had not "met" during the *Planck* QM activity and so this integration was performed for the first time during the *Planck* PFM campaign. The integration process had undergone much study and required special rotatable ground support equipment (GSE) for the LFI RAA, and a special suspension and balancing system to allow HFI to be lifted and lowered into LFI at the correct orientation along guide rails from above. Fortunately the integration was completed successfully.

Subsequently, the combined LFI RAA and HFI FPU were integrated onto the satellite, supported by the LFI GSE, which was eventually removed during integration to the telescope. The process of electrical integration and checkout was then completed for LFI, the SCS and HFI, and the protoflight model test campaign commenced.

For LFI, this test campaign proceeded with ambient functional checkout followed by detailed tests (as a complete subsystem prior to participation with the SCS and HFI in the sequence of alignment), electromagnetic compatibility (EMC), sine and random acoustic vibration tests, and the sequence of system level verification tests with the Mission Operations Control Centre (MOC, at ESOC, Darmstadt) and LFI DPC. During all of these tests, at key points, both the nominal and redundant SCS were put through ambient temperature health checks to verify basic functionality.

The environmental test campaign culminated with the thermal balance and cryogenic tests carried out at the Focal 5 facility of the Centre Spatial de Liège, Belgium. The test was designed to follow very closely the expected cool-down scenario after launch through to normal mission operations, and it was during these tests that the two instruments and the sorption cooler directly demonstrated together not only their combined capabilities but also successfully met their operational margins.

5. LFI test and verification

The LFI had been tested and calibrated before launch at various levels of integration, from the single components up to instrument and satellite levels; this approach, which is summarised schematically in Fig. 11, provided inherent redundancy and optimal instrument knowledge.

Table 4. Measured performance parameters of the LFI passive components.

Feed Horns	Return Loss[1] , Cross-polar (±45°) and Co-polar patterns (E, H and ±45° planes) in amplitude and phase, Edge taper at 22°
OMTs	Insertion Loss, Return Loss, Cross-polarisation, Isolation
Waveguides	Insertion Loss, Return Loss, Isolation

Notes. (1) Return loss and patterns (E, H for all frequencies, also ±45° and cross-polar for the 70 GHz system) have been measured for the assembly Feed Horn + OMT as well.

Passive components, i.e., feed-horns, OMTs, and waveguides, were tested at room conditions at the Plasma Physics Institute of the National Research Council (IFP-CNR) using a Vector Network Analyser. A summary of the measured performance parameters is provided in Table 4; measurements and results are discussed in detail in Villa et al. (2009) and D'Arcangelo et al. (2009a,b).

In addition, radiometric performance was measured several times during the LFI development on individual subunits (e.g., amplifiers, phase switches, detector diodes) on integrated front-end and back-end modules (Davis et al. 2009; Artal et al. 2009; Varis et al. 2009) and on the complete radiometric assemblies, both as independent RCAs (Villa et al. 2010) and in RAA, the final integrated instrument configuration (Mennella et al. 2010).

In Table 5 (taken from Mennella et al. 2010), we list the main LFI radiometric performance parameters and the integration levels at which they have been measured. After the flight instrument test campaign, the LFI was cryogenically tested again after integration on the satellite with the HFI, while the final characterisation will be performed in-flight before starting nominal operations.

The RCA and RAA test campaigns have been important to characterizing the instrument functionality and behaviour, and measuring its expected performance in flight conditions. In particular, 30 GHz and 44 GHz RCAs were integrated and tested in Italy, at the Thales Alenia Space (TAS-I) laboratories in Milan, while the 70 GHz RCA test campaign was carried out in Finland at the Yilinen-Elektrobit laboratories (Villa et al. 2010). After this testing phase, the 11 RCAs were collected and integrated with the flight electronics in the LFI main frame at the TAS-I labs, where the instrument final test and calibration has taken place (Mennella et al. 2010). Custom-designed cryofacilities (Terenzi et al. 2009b; Morgante et al., in prep.) and high-performance black-body input loads (Terenzi et al. 2009a; Cuttaia et al. 2009) were developed to test the LFI in the most flight-representative environmental conditions.

A particular point must be made about the front-end bias tuning, which is a key step in determining the instrument scientific performance. Tight mass and power constraints called for a simple design of the DAE box so that power bias lines were divided into five common-grounded power groups with no bias voltage readouts. Only the total drain current flowing through the front-end amplifiers is measured and is available to the housekeeping telemetry.

This design has important implications for front-end bias tuning, which depends critically on the satellite electrical and thermal configuration. Therefore, this step was repeated at all integration stages and will also be repeated during ground satellite tests and in-flight before the start of nominal operations. Details about the bias tuning performed on front-end modules and on the individual integrated RCAs can be found in Davis et al. (2009), Varis et al. (2009), and Villa et al. (2010).

Table 5. Main calibration parameters and where they have been/will be measured.

Category	Parameters	RCA	RAA	SAT	FLI
Tuning	FE LNAs	Y	Y	Y	Y
	FE PS	Y	Y	Y	Y
	BE offset and gain	Y	Y	Y	Y
	Quantisation/compression	N	Y	Y	Y
Radiom.	Photometric calibration	Y	Y	Y	Y
	Linearity	Y	Y	Y	Y
	Isolation	Y	Y	Y	Y
	In-band response	Y	N	N	N
Noise	White noise	Y	Y	Y	Y
	Knee freq.	Y	Y	Y	Y
	$1/f$ slope	Y	Y	Y	Y
Susc.	FE temperature fluctuations	Y	Y	Y	Y
	BE temperature fluctuations	Y	Y	N	N
	FE bias fluctuations	Y	Y	N	N

Notes. The following abbreviations have been used: SAT = Satellite; FLI = In-flight; FE = Front-end; BE = Back-end; LNA = Low noise amplifier; PS = Phase switch; Radiom = Radiometric; and Susc = Susceptibility.

Table 6. Calibrated white noise from ground-test results extrapolated to the CMB input signal level.

Frequency channel	30 GHz	44 GHz	70 GHz
White noise per ν channel $[\mu K \cdot \sqrt{s}]$	141–154	152–160	130–146

Notes. Two different methods are used to provide a reliable range of values (see Mennella et al. 2010, for further details). The final verification of sensitivity will be derived in-flight during the commissioning performance verification (CPV) phase.

Parameters measured on the integrated instrument were found to be essentially in line with measurements performed on individual receivers; in particular, the LFI shows excellent $1/f$ stability and rejection of instrumental systematic effects. On the other hand, the very ambitious sensitivity goals have not been fully met and the white noise sensitivity (see Table 6) is ~30% higher than requirements. Nevertheless, the measured performance makes LFI the most sensitive instrument of its kind, a factor of 2 to 3 superior to WMAP[8] at the same frequencies.

6. LFI data processing centre (DPC)

To take maximum advantage of the capabilities of the *Planck* mission and achieve its very ambitious scientific objectives, proper data reduction and scientific analysis procedures were defined, designed, and implemented very carefully. The data processing was optimized so as to extract the maximum amount of useful scientific information from the data set and deliver the calibrated data to the broad scientific community within a rather short period of time. As demonstrated by many previous space missions using state-of-the-art technologies, optimal scientific exploitation is obtained by combining the robust, well-defined architecture of a data pipeline and its associated tools with the high scientific creativity essential when facing unpredictable

[8] Calculated on the final resolution element per unit integration time.

features of the real data. Although many steps required for the transformation of data were defined during the development of the pipeline, since most of the foreseeable ones have been implemented and tested during simulations, some of them will remain unknown until flight data are obtained.

Planck is a PI mission, and its scientific achievements will depend critically on the performance of the two instruments, LFI and HFI, on the cooling chain, and on the telescope. The data processing will be performed by two DPCs (Pasian et al. 2000; Pasian & Gispert 2000; Pasian & Sygnet 2002). However, despite the existence of two separate distributed DPCs, the success of the mission relies heavily on the combination of the measurements from both instruments.

The development of the LFI DPC software has been performed in a collaborative way across a consortium spread over 20 institutes in a dozen countries. Individual scientists belonging to the software prototyping team have developed prototype codes, which have then been delivered to the LFI DPC integration team. The latter is responsible for integrating, optimizing, and testing the code, and has produced the pipeline software to be used during operations. This development takes advantage of tools defined within the *Planck* IDIS (integrated data and information system) collaboration.

A software policy has defined, to allow the DPC perform the best most superior algorithms within its pipeline, while fostering collaboration inside the LFI consortium and across *Planck*, and preserving at the same time the intellectual property of the code authors on the processing algorithms devised.

The *Planck* DPCs are responsible for the delivery and archiving of the following scientific data products, which are the deliverables of the *Planck* mission:

- Calibrated time series data, for each receiver, after removal of systematic features and attitude reconstruction.
- Photometrically and astrometrically calibrated maps of the sky in each of the observed bands.
- Sky maps of the main astrophysical components.
- Catalogues of sources detected in the sky maps of the main astrophysical components.
- CMB power spectrum coefficients and an associated likelihood code.

Additional products, necessary for the total understanding of the instrument, are being negotiated for inclusion in the *Planck* Legacy Archive (PLA). The products foreseen to be added to the formally defined products mentioned above are:

- Data sets defining the estimated characteristics of each detector and the telescope (e.g. detectivity, emissivity, time response, main beam and side lobes, etc.).
- "Internal" data (e.g. calibration data-sets, data at intermediate level of processing).
- Ground calibration and assembly integration and verification (AIV) databases produced during the instrument development; and by gathering all information, data, and documents relative to the overall payload and all systems and subsystems. Most of this information is crucial for processing flight data and updating the knowledge and performance of the instrument.

The LFI DPC processing can be logically divided into three levels:

- Level 1: includes monitoring of instrument health and behaviour and the definition of corrective actions in the case of unsatisfactory function, and the generation of time ordered information (TOI, a set of ordered information on either a temporal or scan-phase basis), as well as data display, checking, and analysis tools.
- Level 2: TOIs produced at Level 1 will be cleaned by removing noise and many other types of systematic effects on the basis of calibration information. The final product of the Level 2 includes "frequency maps".
- Level 3: "component maps" will be generated by this level through a decomposition of individual "frequency maps" and by also using products from the other instrument and, possibly, ancillary data.

One additional level ("Level S") is also implemented to develop the most sophisticated simulations based on true instrument parameters extracted during the ground test campaigns.

In the following sections, we describe the DPC Levels and the software infrastructure, and we finally report briefly on the tests that were applied to ensure that all pipelines are ready for the launch.

6.1. DPC Level 1

Level 1 takes input from the MOC's data distribution system (DDS), decompresses the raw data, and outputs time ordered information for Level 2. Level 1 does not include scientific processing of the data; actions are performed automatically by using pre-defined input data and information from the technical teams. The inputs to Level 1 are telemetry (TM) and auxiliary data as they are released by the MOC. Level 1 uses TM data to perform a routine analysis (RTA – real time assessment) of the spacecraft and instrument status, in addition to what is performed at the MOC, with the aim of monitoring the overall health of the payload and detecting possible anomalies. A quick-look data analysis (TQL – telemetry quick look) of the science TM is also done, to monitor the operation of the observation plan and verify the performance of the instrument. This processing is meant to lead to the full mission raw-data stream in a form suitable for subsequent data processing by the DPC.

Level 1 also deals with all activities related to the production of reports. This task includes the results of telemetry analysis, but also the results of technical processing carried out on TOI to understand the current and foreseen behaviour of the instrument. This second item includes specific analysis of instrument performance (LIFE – LFI Integrated perFormance Evaluator), and more general checking of time series (TSA – time series analysis) for trend analysis purposes and comparison with the TOI from the other instrument. The additional tasks of Level 1 relate to its role as an instrument control and DPC interface with the MOC. In particular, the following actions are performed:

- Preparation of telecommanding procedures aimed at modifying the instrument setup.
- Preparation of Mission Information dataBases (MIBs).
- Communicate to the MOC "longer-term" inputs derived from feedback from DPC processing.
- Calibration of REBA parameters to fit long-term trends in the instrument setup.

In Level 1, all actions are planned to be performed on a "day-to-day" basis during operation. In Fig. 12, the structure of Level 1 and required timings are shown. For more details, we refer to Zacchei et al. (2009).

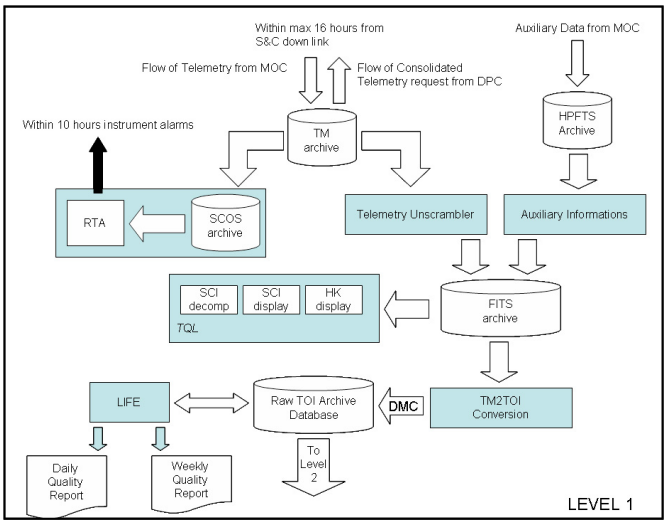

Fig. 12. Level 1 structure.

6.2. DPC Level 2

At this level, data processing steps requiring detailed instrument knowledge (data reduction proper) will be performed. The raw time series from Level 1 will also be used to reconstruct a number of calibrated scans for each detector, as well as instrumental performance and properties, and maps of the sky for each channel. This processing is iterative, since simultaneous evaluation of quite a number of parameters should be made before the astrophysical signal can be isolated and averaged over all detectors in each frequency channel. Continuous exchange of information between the two DPCs will be necessary at Level 2 to identify any suspect or unidentified behaviour or any results from the detectors.

The first task that the Level 2 performs is the creation of differenced data. Level 1 stores data from both Sky and Load. These two have to be properly combined to produce differenced data, therefore reducing the impact of $1/f$ noise achieved by computing the so-called gain modulation factor R, which is derived by taking the ratio of the mean signals from both Sky and Load.

After differenced data are produced, the next step is the photometric calibration that transforms the digital units into physical units. This operation is quite complex: different methods are implemented in the Level 2 pipeline that use the CMB dipole as an absolute calibrator allowing for the conversion into physical units.

Another major task is beam reconstruction, which is implemented using information from planet crossings. An algorithm was developed that performs a bi-variate approximation of the main beam section of the antenna pattern and reconstructs the position of the horn in the focal plane and its orientation with respect to a reference axis.

The step following the production of calibrated timelines is the creation of calibrated frequency maps. To achieve this, pointing information will be encoded into time-ordered pixels i.e., pixel numbers in the given pixelisation scheme (HEALPix) by identifying a given pointing direction that is ordered in time. To produce temperature maps, it is necessary to reconstruct the beam pattern along the two polarisation directions for the main, intermediate, and far parts of the beam pattern. This will allow the combination of the two orthogonal components into a single temperature timeline. On this temperature timeline, a map-making algorithm will be applied to produce a map from each receiver.

The instrument model allows one to check and control systematic effects and the quality of the removal performed by map-making and calibration of the receiver map. Receiver maps cleaned of systematic effects at different levels of accuracy will be stored into a calibrated map archive. The production of frequency-calibrated maps will be performed by processing together all receivers from a given frequency channel in a single map-making run. In Figs. 13 and 14, we report the steps performed by Level 2, together with the associated times foreseen.

6.3. DPC Level 3

The goal of the DPC Level 3 is to estimate and characterise maps all the different astrophysical and cosmological sources of emission ("components") present at *Planck* wavelengths. Using the CMB component obtained after point-source extraction and cleaning from diffuse, Galactic emission, the APS of the CMB is estimated for temperature, polarisation, and cross temperature/polarisation modes.

The extraction of the signal from Galactic point-like objects, and other galaxies and clusters is achieved as a first step, either using pre-existing catalogues based on non-*Planck* data, or filtering the multi-frequency maps with optimal filters to detect and identify beam-like objects (see Herranz et al. 2009, and references therein).

The algorithms dedicated to the separation of diffuse emission fall into four main categories, depending on the criteria exploited to achieve separation, and making use of the wide frequency coverage of *Planck* (see Leach et al. 2008, and references therein). Internal linear combination and template fitting achieves linear mixing and combination of the multi-frequency data with other data sets, optimized for CMB or foreground recovery. The independent component analysis works in the statistical domain, without using foreground modelling or spatial correlations in the data, but assuming instead statistical independence between the components that are to be recovered. The correlated component analysis, on the other hand, makes use of a parametrization of foreground unknowns, and uses spatial correlations to achieve separation. Finally, parametric methods consist of modelling foreground and CMB components by treating each resolution element independently, achieving fitting of the unknowns and separation by means of a maximum likelihood analysis. The LFI DPC Level 3 includes algorithms that belong to each of the four categories outlined above. The complementarity of different methods for different purposes, as well as the cross-check on common products, are required to achieve reliable and complete scientific products.

As for power spectrum estimation, two independent and complementary approaches have been implemented (see Gruppuso et al. 2009, and references therein): a Monte-Carlo method suitable for high multipoles (based on the MASTER approach, but including cross-power spectra from independent receivers); and a maximum likelihood method for low multipoles. A combination of the two methods will be used to produce the final estimation of the APS from LFI data, before its combination with HFI data. In Fig. 15, we report the steps performed in the Level 3 pipeline with the associated timescales foreseen.

The inputs to the Level 3 pipeline are the three calibrated frequency maps from LFI together with the six calibrated HFI frequency maps that should be exchanged on a monthly basis. The Level 3 pipeline has links with most of the stages of the Level 1

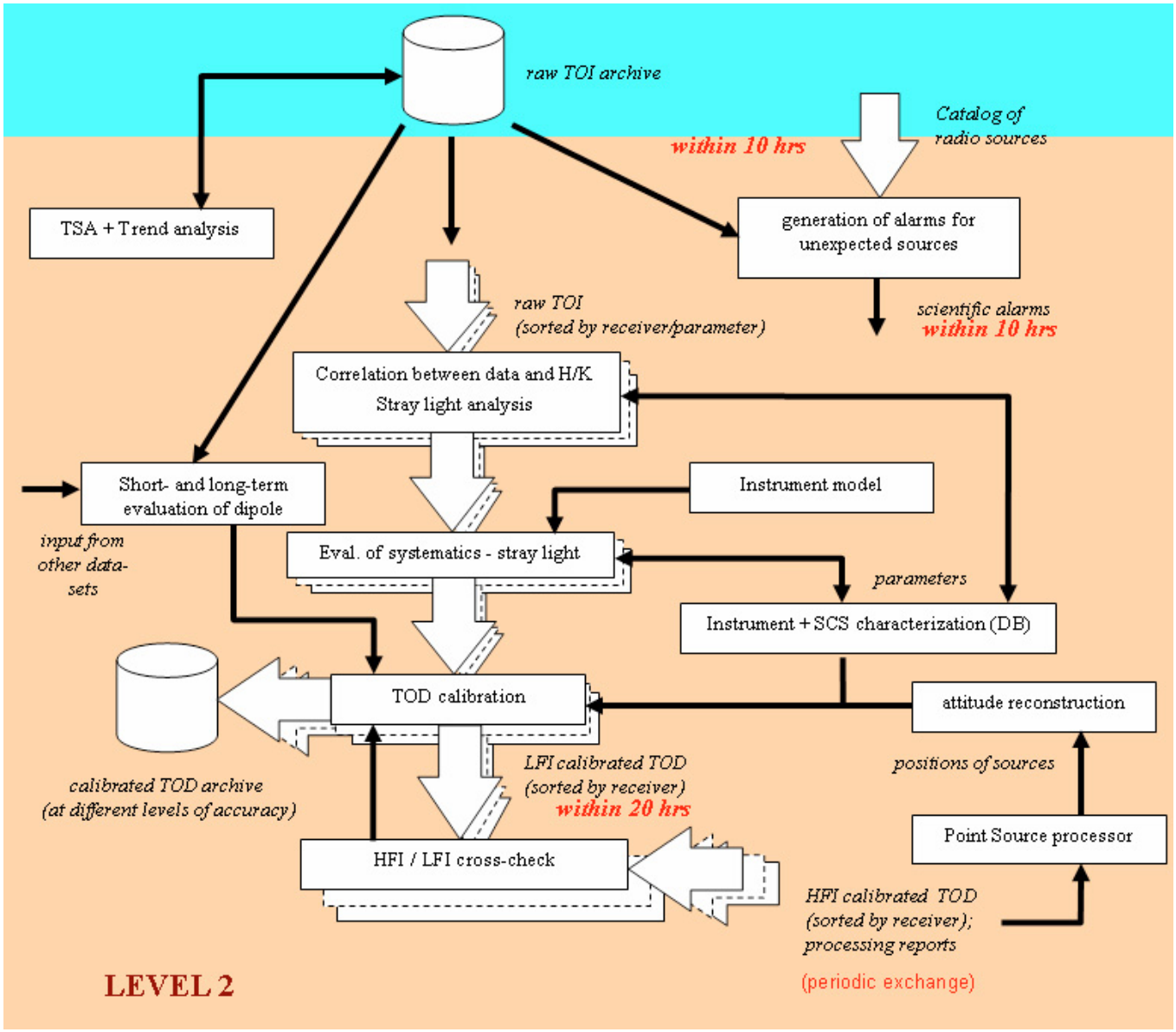

Fig. 13. Level 2 calibration pipeline.

and Level 2 pipelines, and therefore the most complete and detailed knowledge of the instrumental behaviour is important for achieving its goals. Systematic effects appearing in the time-ordered data, beam shapes, band width, source catalogues, noise distribution, and statistics are examples of important inputs to the Level 3 processing. Level 3 will produce source catalogues, component maps, and CMB power spectra that will be delivered to the PLA, together with other information and data needed for the public release of the *Planck* products.

6.4. DPC Level S

It was widely agreed within both consortia that a software system capable of simulating the instrument footprint, starting from a predefined sky, was indispensable for the full period of the *Planck* mission. Based on that idea, an additional processing level, Level S, was developed and upgraded whenever the knowledge of the instrument improved (Reinecke et al. 2006). Level S now incorporates all the instrument characteristics as they were understood during the ground test campaign. Simulated data were used to evaluate the performance of data-analysis algorithms and software against the scientific requirements of the mission and to demonstrate the capability of the DPCs to work using blind simulations that contain unknown parameter values to be recovered by the data processing pipeline.

6.5. DPC software infrastructure

During the entire *Planck* project, it has been (and will continue to be) necessary to deal with aspects related to information management, which pertain to a variety of activities concerning the whole project, ranging from instrument information (e.g., technical characteristics, reports, configuration control documents, drawings, public communications) to software development/control (including the tracking of each bit produced by each pipeline). For this purpose, an integrated data and information system (IDIS) was developed. IDIS (Bennett et al. 2000) is a collection of software infrastructure

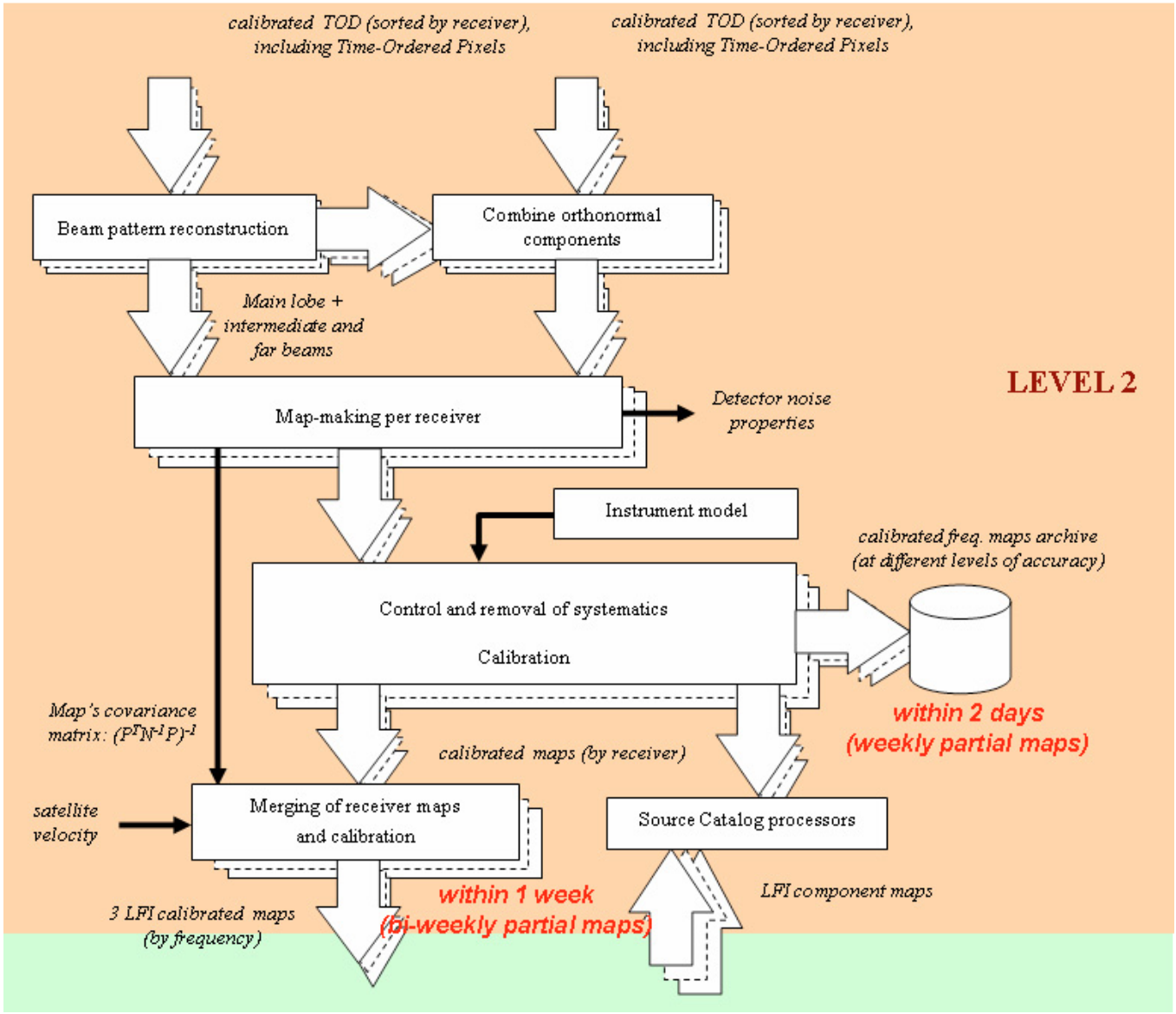

Fig. 14. Level 2 Map-making pipeline.

for supporting the *Planck* DPCs in their management of large quantities of software, data, and ancillary information. The infrastructure is relevant to the development, operational, and post-operational phases of the mission.

The full IDIS can be broken down into five major components:

- Document management system (DMS), to store and share documents.
- Data management component (DMC), allowing the ingestion, efficient management, and extraction of the data (or subsets thereof) produced by *Planck* activities.
- Software component (SWC), allowing the system to administer, document, handle, and keep under configuration control the software developed within the *Planck* project.
- Process Coordinator (ProC), allowing the creation and running of processing pipelines inside a predefined and well controlled environment.
- Federation layer (FL), which allows controlled access to the previous objects and acts as a glue between them.

The use of the DMS has allowed the entire consortia to ingest and store hundreds of documents and benefit from an efficient way of retrieving them. The DMC is an API (application programming interface) for data input/output, connected to a database (either relational or object-oriented) and aimed at the archiving and retrieval of data and the relevant meta-information; it also features a user GUI. The ProC is a controlled environment in which software modules can be added to create an entirely functional pipeline. It stores all the information related to versioning of the modules used, data, and temporary data created within the database while using the DMC API. In Fig. 16, an example of the LFI pipeline is shown. Finally, the FL is an API that, using a remote LDAP database, assigns the appropriate permission to the users for data access, software access, and pipeline run privileges.

6.6. DPC test performed

Each pipeline and sub-pipeline (Level 1, Level 2, and Level 3) has undergone different kinds of tests. We report here only the

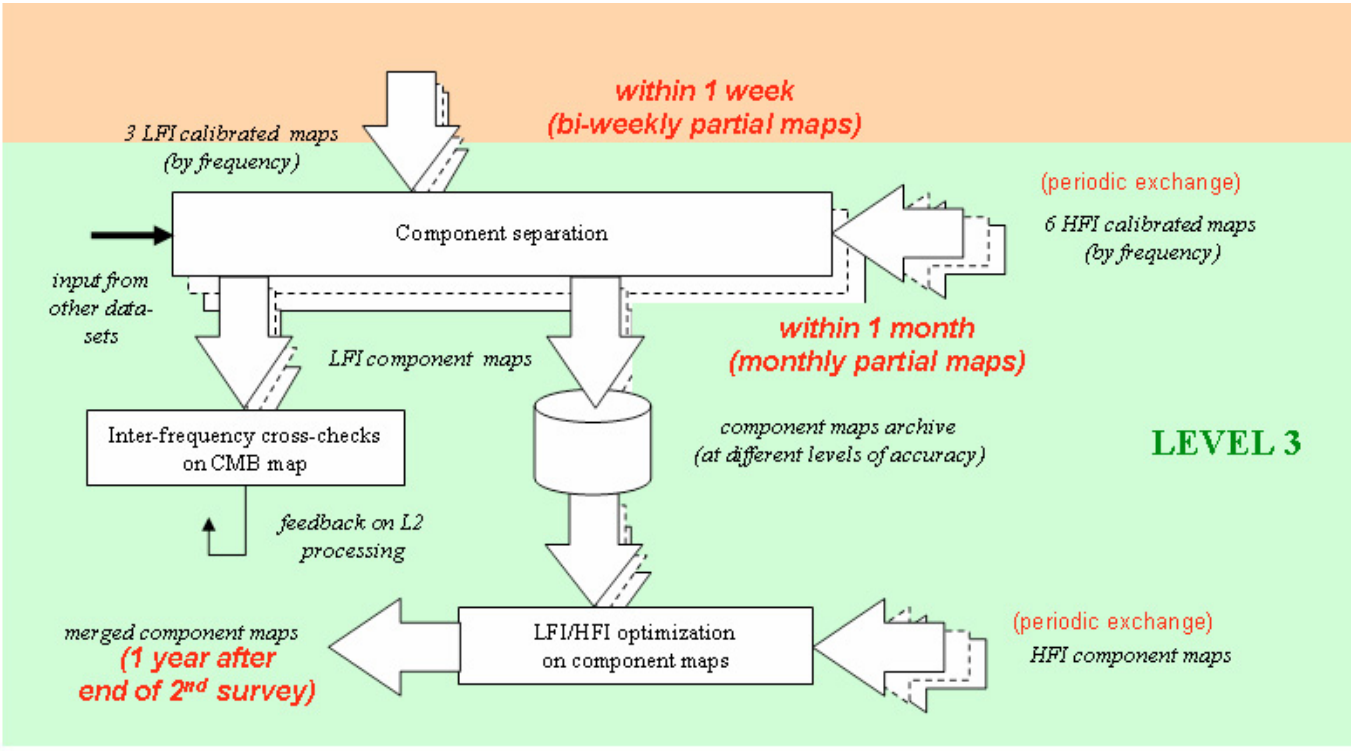

Fig. 15. Level 3 pipeline structure.

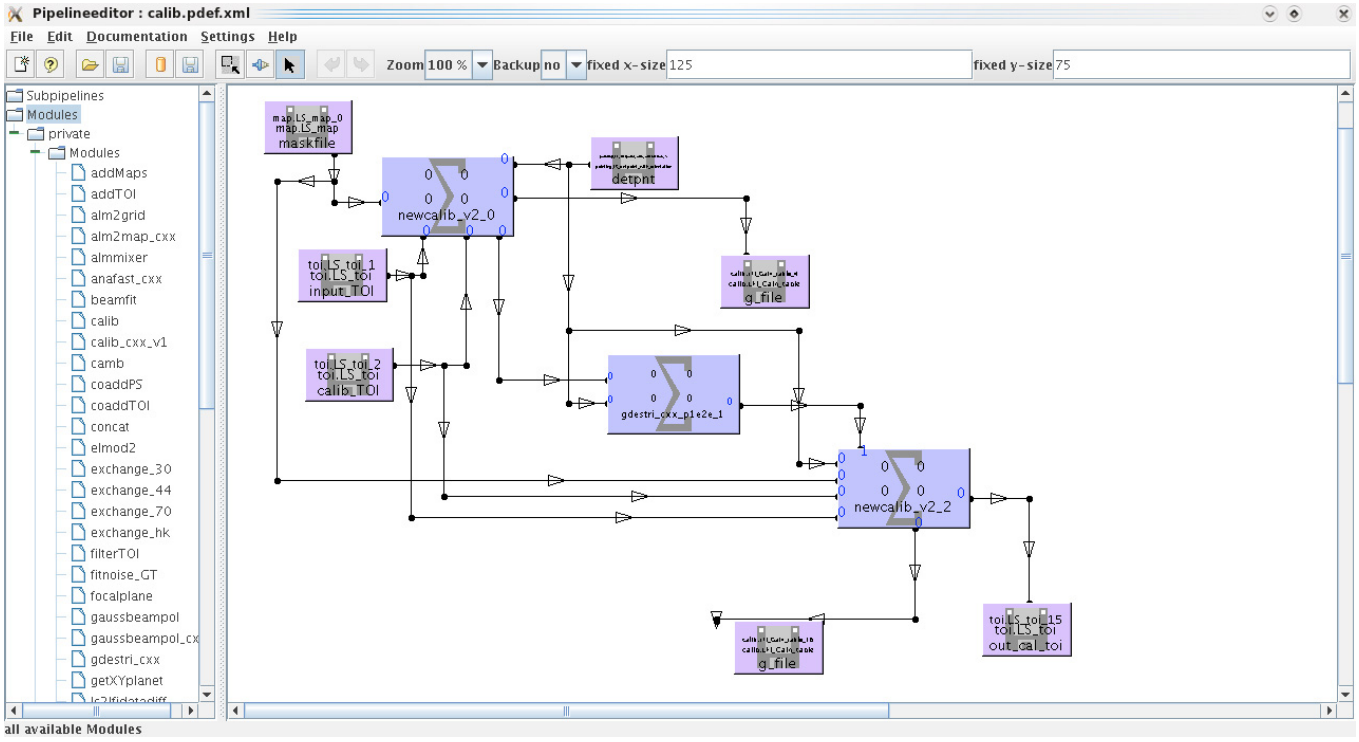

Fig. 16. IDIS ProC pipeline editor.

official tests conducted with ESA, without referring to the internal tests that were dedicated to DPC subsystems. Level 1 was the most heavily tested, as this pipeline is considered launch-critical. As a first step, it was necessary to validate the output with respect to the input; to do that, we ingested inside the instrument a well known signal as described in Frailis et al. (2009) with the purpose of verifying whether the processing inside Level 1 was correct. This also had the benefit of providing an independent test of important functionalities for the REBA software responsible for the onboard preprocessing of scientific data. Afterwards, more complete tests, including all interfaces with other elements of the ground segment, were performed. Those tests simulate

one week of nominal operations (SOVT1 – system operation validation test; Keck 2008) and, during the SOVT2, one week of the commissioning performance verification (CPV) phase. During these tests, it was demonstrated that the LFI Level 1 is able to deal with the telemetry as it would be acquired during operations.

Tests performed on Level 2 and Level 3 were more science-oriented to demonstrate the scientific adequacy of the LFI DPC pipeline, i.e., its ability to produce scientific results commensurate with the objectives of the *Planck* mission. These tests were based on blind simulations of growing complexity. The Phase 1 test data, produced with Level S, featured some simplifying approximations:

- the sky model was based on the "concordance model" CMB (no non-Gaussianity);
- the dipole did not include modulations due to the Lissajous orbit around L2;
- Galactic emission was obtained assuming non-spatially varying spectral index;
- the detector model was "ideal" and did not vary with time;
- the scanning strategy was "ideal" (i.e., no gaps in the data).

The results of this test were in line with the objectives of the mission (see Perrotta & Maino 2007)).

The Phase 2 tests are still ongoing. They take into account more realistic simulations with all the known systematics and known problems (e.g., gaps) in the data.

7. Pre-launch status

We have provided an overview of the LFI programme and of its organization within the ESA *Planck* mission. After a brief description of the *Planck* main properties and observational strategy, the main scientific goals have been presented, ranging from fundamental cosmology to Galactic and extragalactic astrophysics by focusing on those more relevant to LFI. The LFI design and development have been outlined, together with the model philosophy and testing strategy. The LFI approach to on-ground and in-flight calibration and the LFI ground segment have been described. We have reported on the data analysis pipeline that has been successfully tested.

Ground testing shows that the LFI operates as anticipated. The observational program will begin after the *Planck/Herschel* launch on May 14th, 2009.

A challenging commissioning and final calibration phase will prepare the LFI for nominal operations that will start about 90 days after launch. After ~20 days, the instrument will be switched on and its functionality will be tested in parallel with the cooling of the 20 K stage. Then the cooling period of the HFI focal plane to 4 K will be used by the LFI to tune voltage biases of the front end amplifiers, phase switches, and REBA parameters, which will set the final scientific performance of the instrument. Final tunings and calibration will be performed in parallel with HFI activities for about 25 days until the last in-flight calibration phase, the so-called "first light survey". This will involve 14 days of data acquisition in nominal mode that will benchmark the whole system, from satellite and instruments to data transmission, ground segment, and data processing levels.

The first light survey will produce the very first *Planck* maps. This will not be designed for scientific exploitation but will rather serve as a final test of the instrumental and data processing capabilities of the mission. After this, the *Planck* scientific operations will begin.

Note that at the time of publishing this article, Planck was launched successfully with Herschel on May 14th, 2009, and it has completed its first full sky survey as foreseen.

Acknowledgements. *Planck* is a project of the European Space Agency with instruments funded by ESA member states, and with special contributions from Denmark and NASA (USA). The *Planck*-LFI project is developed by an International Consortium led by Italy and involving Canada, Finland, Germany, Norway, Spain, Switzerland, UK and USA. The Italian contribution to *Planck* is supported by the Agenzia Spaziale Italiana (ASI) and INAF. We also wish to thank the many people of the *Herschel/Planck* Project and RSSD of ESA, ASI, THALES Alenia Space Industries and the LFI Consortium that have contributed to the realization of LFI. We are grateful to our HFI colleagues for such a fruitful collaboration during so many years of common work. The German participation at the Max-Planck-Institut für Astrophysik is funded by the Bundesministerium für Wirtschaft und Technologie through the Raumfahrt-Agentur of the Deutsches Zentrum für Luft- und Raumfahrt (DLR) [FKZ: 50 OP 0901] and by the Max-Planck-Gesellschaft (MPG). The Finnish contribution is supported by the Finnish Funding Agency for Technology and Innovation (Tekes) and the Academy of Finland. The Spanish participation is funded by Ministerio de Ciencia e Innovacion through the project ESP2004-07067-C03 and AYA2007-68058-C03. The UK contribution is supported by the Science and Technology Facilities Council (STFC). C. Baccigalupi and F. Perrotta acknowledge partial support of the NASA LTSA Grant NNG04CG90G. We acknowledge the use of the BCX cluster at CINECA under the agreement INAF/CINECA. We acknowledge the use of the Legacy Archive for Microwave Background Data Analysis (LAMBDA). Support for LAMBDA is provided by the NASA Office of Space Science. We acknowledge use of the HEALPix (Górski et al. 2005) software and analysis package for deriving some of the results in this paper. The Canadian participation is supported by the Canadian Space Agency.

Appendix A: List of Acronyms

AIV = assembly integration and verification
API = application programming interface
APS = angular power spectrum
ASI = Agenzia Spaziale Italiana (Italian Space Agency)
ATCA = Australian Telescope Compact Array
AVM = avionics model
BEM = back-end module
BEU = back-end unit
CDM = cold dark matter
COBE = COsmic Background Explorer
COBRAS = COsmic Background Radiation Anisotropy Satellite
CMB = cosmic microwave background
CPV = commissioning performance verification
CSL = Centre Spatial de Liège
DAE = data acquisition electronics
DBI = Dirac-born-infeld (inflation)
DC = direct current
DDS = data distribution system
DMC = data management component
DMS = document management system
DPC = data processing centre
EBB = Elegant BreadBoarding
EMC = electromagnetic compatibility
ESA = European Space Agency
ESOC = European Space Operations Centre
ET = edge taper
FEM = front-end module
FL = federation layer
FM = flight model
FPU = focal plane unit
FWHM = full width half maximum
GLAST = Gamma-ray Large Area Space Telescope
GLS = generalized least squares
GSE = ground support equipment

GUI = graphical user interface
HEALPix = Hierarchical Equal Area isoLatitude Pixelization
HEMT = high electron mobility transistor
HFI = High Frequency Instrument
HPST = high-pressure stabilization tank
IDIS = integrated data and information system
IR = infra red
ISM = inter-stellar medium
JPL = Jet Propulsion Laboratory
JT = Joule-Thomson
LDAP = Lightweight Directory Access Protocol
LFI = Low Frequency Instrument
LIFE = LFI integrated perFormance Evaluator
LNA = low noise amplifier
LPSB = low-pressure storage bed
LVHX = Liquid Vapour Heat eXchange
MIB = mission information base
MIC = microwave integrated circuit
MMIC = monolithic microwave integrated circuit
MOC = mission operation centre
NASA = National Aeronautics and Space Administration (USA)
NG = non Gaussianity
OMT = orthomode transducer
PACE = piping and cold-end assembly
PD = prototype demonstrator
PFM = *Planck* protoflight model
PI = Principal Investigator
PID = proportional integral derivative
PLA = *Planck* Legacy Archive
PPLM = *Planck* PayLoad Module
ProC = Process Coordinator
PS = phase switch
QM = qualification model
RAA = radiometer array assembly
RCA = radiometer chain assembly
REBA = Radiometer Electronics Box Assembly
RF = radio frequency
RTA = real time assessment
SAMBA = SAtellite for Measurement of Background Anisotropies
SCE = sorption cooler electronics
SCS = sorption cooler subsystem
SOVT = system operation validation test
SS = scanning strategy
SVM = SerVice Module
SWC = SoftWare Component
TM = TeleMetry
TMU = thermo-mechanical unit
TOI = time order information
TQL = telemetry quick look
TSA = temperature stabilization assembly; time series analysis
WMAP = Wilkinson Microwave Anisotropy Probe
WR = warm radiator
XPD = cross-polar discrimination

References

Aatrokoski, J., Lähteenmäki, A., Tornikoski, M., et al. 2010, MNRAS, 401, 597
Abdo, A. A. 2009, ApJ, 700, 597
Abramo, L. R., Bernui, A., Ferreira, I. S., Villela, T., & Wuensche, C. A. 2006, Phys. Rev. D, 74, 063506
Alishahiha, M., Silverstein, E., & Tong, D. 2004, Phys. Rev. D, 70, 123505
Artal, E., Aja, B., L. de la Fuente, M., et al. 2009, JINST, 4, T12003
Ashdown, M. A. J., Baccigalupi, C., Balbi, A., et al. 2007, A&A, 467, 761
Ashdown, M. A. J., Baccigalupi, C., Bartlett, J. G., et al. 2009, A&A, 493, 753
Atwood, W. B., Abdo, A. A., Ackermann, M., et al. 2009, ApJ, 697, 1071
Babich, D., & Zaldarriaga, M. 2004, Phys. Rev. D, 70, 083005
Barbosa, D., Bergano, J., Fonseca, R., et al. 2006, in PoS(CMB2006)029, CMB and Physics of the Early Universe, ed. G. de Zotti, et al.
Bartlett, J. G., Chamballu, A., Melin, J.-B., Planck Working Group 5 2008, Astron. Nachr., 329, 147
Bartolo, N., & Riotto, A. 2009, J. Cosmol. Astro-Part. Phys., 3, 17
Bartolo, N., Komatsu, E., Matarrese, S., & Riotto, A. 2004, Phys. Rep., 402, 103
Bennett, K., Pasian, F., Sygnet, J.-F., et al. 2000, in SPIE Conf. Ser. 4011, ed. R. I. Kibrick, & A. Wallander, 2
Bernard, J.-P., Ade, P., de Bernardis, P., et al. 2007, in EAS Publ. Ser., ed. M.-A. Miville-Deschênes, & F. Boulanger, 23, 189
Bersanelli, M., Mattaini, E., Santambrogio, E., et al. 1998, Exper. Astron., 8, 231
Bersanelli, M., Mandolesi, N., Butler, R. C., et al. 2010, A&A, 520, A4
Bhandari, P., Prina, M., Bowman, J., et al. 2004, Advances in Cryogenic Engineering, 44, 395
Bonaldi, A., Ricciardi, S., Leach, S., et al. 2007, MNRAS, 382, 1791
Burigana, C., Malaspina, M., Mandolesi, N., et al. 1997, A preliminary study on destriping techniques of PLANCK/LFI measurements versus observational strategy, Tech. Rep. 198/1997, TeSRE/CNR, Bologna [arXiv:astro-ph/9906360]
Burigana, C., Natoli, P., Vittorio, N., Mandolesi, N., & Bersanelli, M. 2001, Exper. Astron., 12, 87
Burigana, C., Sandri, M., Villa, F., et al. 2004, A&A, 428, 311
Burigana, C., La Porta, L., Reich, W., et al. 2006, in PoS(CMB2006)016, CMB and Physics of the Early Universe, ed. G. de Zotti, et al.
Cho, J., & Lazarian, A. 2003, New Astron. Rev., 47, 1143
Collaudin, B., & Passvogel, T. 1999, Cryogenics, 39, 157
Copi, C. J., Huterer, D., & Starkman, G. D. 2004, Phys. Rev. D, 70, 043515
Copi, C. J., Huterer, D., Schwarz, D. J., & Starkman, G. D. 2007, Phys. Rev. D, 75, 023507
Copi, C. J., Huterer, D., Schwarz, D. J., & Starkman, G. D. 2009, MNRAS, 399, 295
Cremonese, G., Marzari, F., Burigana, C., & Maris, M. 2002, New Astron., 7, 483
Cruz, M., Martínez-González, E., Vielva, P., & Cayón, L. 2005, MNRAS, 356, 29
Cumberbatch, D. T., Zuntz, J., Kamfjord Eriksen, H. K., & Silk, J. 2009 [arXiv:0902.0039]
Cuttaia, F., Mennella, A., Stringhetti, L., et al. 2009, JINST, 4, T12013
Dallacasa, D., Stanghellini, C., Centonza, M., & Fanti, R. 2000, A&A, 363, 887
D'Arcangelo, O., Battaglia, P., Bersanelli, M., et al. 2005, Performance of the *Planck*-LFI feed horns Qualification Model
D'Arcangelo, O., Figini, L., Simonetto, A., et al. 2009a, JINST, 4, T12007
D'Arcangelo, O., Simonetto, A., Figini, L., et al. 2009b, JINST, 4, T12005
Davis, R., Wilkinson, A., Davies, R., et al. 2009, JINST, 4, T12002
de Gasperis, G., Balbi, A., Cabella, P., Natoli, P., & Vittorio, N. 2005, A&A, 436, 1159
de Zotti, G., Ricci, R., Mesa, D., et al. 2005, A&A, 431, 893
Dobler, G., Draine, B. T., & Finkbeiner, D. P. 2009, Phys. Rev. D, 80, 123518
Draine, B. T., & Lazarian, A. 1998, ApJ, 494, L19
Dunkley, J., Komatsu, E., Nolta, M. R., et al. 2009, ApJS, 180, 306
Dupac, X., & Tauber, J. 2005, A&A, 430, 363
Efstathiou, G. 2004, MNRAS, 349, 603
Efstathiou, G., & Gratton, S. 2009, JCAP, 06, 011
Eriksen, H. K., Hansen, F. K., Banday, A. J., Górski, K. M., & Lilje, P. B. 2004a, ApJ, 605, 14
Eriksen, H. K., Hansen, F. K., Banday, A. J., Górski, K. M., & Lilje, P. B. 2004b, ApJ, 609, 1198
Frailis, M., Maris, M., Zacchei, A., et al. 2009, JINST, 4, T12021
Gentili, G., Nesti, R., Peolsi, G., & Natale, V. 2000, Electr. Lett., 36, 486
Gold, B., Bennett, C. L., Hill, R. S., et al. 2009, ApJS, 180, 265
Gorski, K. M. 1994, ApJ, 430, L85
Górski, K. M., Hivon, E., Banday, A. J., et al. 2005, ApJ, 622, 759
Gruppuso, A., De Rosa, A., Cabella, P., et al. 2009, MNRAS, 400, 463
Hamimeche, S., & Lewis, A. 2008, Phys. Rev. D, 77, 103013
Hansen, F. K., Banday, A. J., & Górski, K. M. 2004, MNRAS, 354, 641
Haverkorn, M., Carretti, E., McConnell, D., et al. 2007, in BAAS, 38, 123
Herranz, D., López-Caniego, M., Sanz, J. L., & González-Nuevo, J. 2009, MNRAS, 394, 510
Hildebrandt, S. R., Rebolo, R., Rubiño-Martín, J. A., et al. 2007, MNRAS, 382, 594
Hinshaw, G., Banday, A. J., Bennett, C. L., et al. 1996, ApJ, 464, L17
Holman, R., & Tolley, A. J. 2008, J. Cosmol. Astro-Part. Phys., 5, 1
Hooper, D., Finkbeiner, D. P., & Dobler, G. 2007, Phys. Rev. D, 76, 083012

Hooper, D., Zaharijas, G., Finkbeiner, D. P., & Dobler, G. 2008, Phys. Rev. D, 77, 043511
Janssen, M. A., & Gulkis, S. 1992, in The Infrared and Submillimetre Sky after COBE, ed. M. Signore, & C. Dupraz, NATO ASIC Proc., 359, 391
Jewell, J., Levin, S., & Anderson, C. H. 2004, ApJ, 609, 1
Keck, F. 2008, *Planck* SOVT1 Test Report, Tech. Rep. PT-PMOC-OPS-RP-6414-OPS-OAP, ESOC Documentation
Keihänen, E., Kurki-Suonio, H., & Poutanen, T. 2005, MNRAS, 360, 390
Keihänen, E., Keskitalo, R., Kurki-Suonio, H., Poutanen, T., & Sirviö, A.-S. 2010, A&A, 520, A8
Keskitalo, R., Ashdown, M. A. J., Cabella, P., et al. 2010, A&A, accepted
Knox, L. 1995, Phys. Rev. D, 52, 4307
Kogut, A., Fixsen, D. J., Levin, S. M., et al. 2009, ApJ, submitted [arXiv:0901.0562]
Komatsu, E., Dunkley, J., Nolta, M. R., et al. 2009, ApJS, 180, 330
Kurki-Suonio, H., Keihanen, E., Keskitalo, R., et al. 2009, A&A, 506, 1511
La Porta, L., Burigana, C., Reich, W., & Reich, P. 2008, A&A, 479, 641
Lamarre, J. M., Puget, J.-L., Ade, P. A. R., et al. 2010, A&A, 520, A9
Land, K., & Magueijo, J. 2005, Phys. Rev. Lett., 95, 071301
Lazarian, A., & Finkbeiner, D. 2003, New Astron. Rev., 47, 1107
Leach, S. M., Cardoso, J.-F., Baccigalupi, C., et al. 2008, A&A, 491, 597
Leahy, J. P., Bersanelli, M., D'Arcangelo, O., et al. 2010, A&A, 520, A8
Lin, Y.-T., Partridge, B., Pober, J. C., et al. 2009, ApJ, 694, 992
Lineweaver, C. H., Smoot, G. F., Bennett, C. L., et al. 1994, ApJ, 436, 452
Maino, D., Burigana, C., Maltoni, M., et al. 1999, A&AS, 140, 383
Mandolesi, N., Smoot, G. F., & Bersanelli, M. 1994, in Present and Future of the Cosmic Microwave Background, ed. J. L. Sanz, E. Martinez-Gonzalez, & L. Cayon (Berlin: Springer Verlag), Lecture Notes in Physics, 429, 228
Mandolesi, N., Bersanelli, M., Burigana, C., et al. 2000, A&AS, 145, 323
Maris, M., & Burigana, C. 2009, Earth, Moon, & Planets, 105, 81
Maris, M., Bersanelli, M., Burigana, C., et al. 2006a, Mem. Soc. Astron. Ital. Suppl., 9, 460
Maris, M., Burigana, C., & Fogliani, S. 2006b, A&A, 452, 685
Marsden, G., Ade, P. A. R., Benton, S., et al. 2008, in SPIE Conf., Ser., 7020
Massardi, M., López-Caniego, M., González-Nuevo, J., et al. 2009, MNRAS, 392, 733
Mennella, A., Bersanelli, M., Burigana, C., et al. 2002, A&A, 384, 736
Mennella, A., Bersanelli, M., Butler, R. C, et al. 2010, A&A, 520, A5
Miville-Deschênes, M.-A., & Lagache, G. 2005, ApJS, 157, 302
Morgante, G., Pearson, D., Stassi, P., et al. 2009, JINST, 4, T12016
Natoli, P., de Gasperis, G., Gheller, C., & Vittorio, N. 2001, A&A, 372, 346
Pasian, F., & Gispert, R. 2000, Astrophys. Lett. Commun., 37, 247
Pasian, F., & Sygnet, J.-F. 2002, in SPIE Conf. Ser. 4847, ed. J.-L. Starck, & F. D. Murtagh, 25
Pasian, F., Bersanelli, M., & Mandolesi, N. 2000, Baltic Astron., 9, 511
Pearson, T. J., & C-BASS collaboration 2007, in BAAS, 38, 883
Pelkonen, V.-M., Juvela, M., & Padoan, P. 2007, A&A, 461, 551
Perrotta, F., & Maino, D. 2007, *Planck* LFI – SGS2 End-to-End test report, Tech. Rep. PL-LFI-OAT-RP-010, LFI DPC Documentation
Ponthieu, N., Macías-Pérez, J. F., Tristram, M., et al. 2005, A&A, 444, 327
Poutanen, T., de Gasperis, G., Hivon, E., et al. 2006, A&A, 449, 1311
Reinecke, M., Dolag, K., Hell, R., Bartelmann, M., & Enßlin, T. A. 2006, A&A, 445, 373
Rubino-Martin, J. A., Rebolo, R., Tucci, M., et al. 2008 [arXiv:0810.3141]
Sandri, M., Villa, F., Nesti, R., et al. 2004, A&A, 428, 299
Sandri, M., Villa, F., Bersanelli, M., et al. 2010, A&A, 520, A7
Schwarz, D. J., Starkman, G. D., Huterer, D., & Copi, C. J. 2004, Phys. Rev. Lett., 93, 221301
Scott, D., & Smoot, G. 2008, in Rev. Part. Phys., 667, 246
Senatore, L., Smith, K. M., & Zaldarriaga, M. 2010, JCAP, 01, 028
Smith, K. M., Senatore, L., & Zaldarriaga, M. 2009, Jour. of Cosmo. & Astrophysics, 09, 006
Smoot, G. F., Bennett, C. L., Kogut, A., et al. 1992, ApJ, 396, L1
Tauber, J. A., Pace, O., & Volonte, S. 1994, ESA, 18, 239
Tauber, J. A., Mandolesi, N., Puget, J.-L., et al. 2010, A&A, 520, A1
Tegmark, M. 1997, ApJ, 480, L87
Tegmark, M., de Oliveira-Costa, A., & Hamilton, A. J. 2003, Phys. Rev. D, 68, 123523
Terenzi, L., Salmon, M. J., Colin, A., et al. 2009a, JINST, 4, T12012
Terenzi, L., Lapolla, M., Laaninen, M., et al. 2009b, JINST, 4, T12015
The Planck Collaboration 2006 [arXiv:astro-ph/0604069]
Umana, G., Burigana, C., & Trigilio, C. 2006, Mem. Soc. Astron. Ital. Suppl., 9, 279
Valenziano, L., Villa, F., Mandolesi, N., & Bersanelli, M. 1998, Focal Surface Evaluation for the *Planck* Telescope, Tech. Rep. 224/1998, TeSRE/CNR, Bologna
Valenziano, L., Cuttaia, F., De Rosa, A., et al. 2009, JINST, 4, T12006
Varis, J., Hughes, N., Laaninen, M., et al. 2009, JINST, 4, T12001
Vielva, P., Martínez-González, E., Barreiro, R. B., Sanz, J. L., & Cayón, L. 2004, ApJ, 609, 22
Vielva, P., Wiaux, Y., Martínez-González, E., & Vandergheynst, P. 2007, MNRAS, 381, 932
Villa, F., Burigana, C., & Mandolesi, N. 1998, A Note on the *Planck* Aplanatic Telescope, Tech. Rep. 221/1998, TeSRE/CNR, Bologna
Villa, F., Sandri, M., Mandolesi, N., et al. 2002, Exp. Astron., 14, 1
Villa, F., D'Arcangelo, O., Pecora, M., et al. 2009, JINST, 4, T12004
Villa, F., Terenzi, L., Sandri, M., et al. 2010, A&A, 520, A6
Wade, L., Bhandari, P., Bowman, J., et al. 2000, Advances in Cryogenic Engineering, 45
Waelkens, A., Jaffe, T., Reinecke, M., Kitaura, F. S., & Enßlin, T. A. 2009, A&A, 495, 697
Wandelt, B. D., Larson, D. L., & Lakshminarayanan, A. 2004, Phys. Rev. D, 70, 083511
Wiaux, Y., Vielva, P., Martínez-González, E., & Vandergheynst, P. 2006, Phys. Rev. Lett., 96, 151303
Wright, E. L., Hinshaw, G., & Bennett, C. L. 1996, ApJ, 458, L53
Wright, E. L., Chen, X., Odegard, N., et al. 2009, ApJS, 180, 283
Yadav, A. P. S., Komatsu, E., & Wandelt, B. D. 2007, ApJ, 664, 680
Zacchei, A., Frailis, M., Maris, M., et al. 2009, JINST, 4, T12019

[1] INAF – IASF Bologna, Istituto Nazionale di Astrofisica, Istituto di Astrofisica Spaziale e Fisica Cosmica di Bologna, via Gobetti 101, 40129 Bologna, Italy, e-mail: mandolesi@iasfbo.inaf.it
[2] Dipartimento di Fisica, Università degli Studi di Milano, via Celoria, 16, 20133 Milano, Italy
[3] INAF – OAPd, Istituto Nazionale di Astrofisica, Osservatorio Astronomico di Padova, Vicolo dellOsservatorio 5, 35122 Padova, Italy
[4] Dipartimento di Fisica G. Galilei, Università degii Studi di Padova, via Marzolo 8, 35131 Padova, Italy
[5] Dipartimento di Fisica, Università degli Studi di Roma "Tor Vergata", via della Ricerca Scientifica 1, 00133 Roma, Italy
[6] INAF – OATs, Istituto Nazionale di Astrofisica, Osservatorio Astronomico di Trieste, via G.B. Tiepolo 11, 34131 Trieste, Italy
[7] Dep. Ing. de Comunicaciones (DICOM), Universidad de Cantabria Av. De Los Castros S/N, 39005 Santander, Spain
[8] SISSA/ISAS, Scuola Internazionale di Studi Superiori Avanzati/International Schools for Advanced Studies, Astrophysics Sector, via Beirut 2–4, Sezione di Trieste, 34014 Trieste, Italy
[9] MPA – Max-Planck-Institut für Astrophysik, Karl-Schwarzschild-Str. 1, 85741 Garching, Germany
[10] Jet Propulsion Laboratory, California Institute of Technology 4800 Oak Grove Drive, Pasadena, CA 91109, USA
[11] ISDC Data Centre for Astrophysics, University of Geneva, ch. d'Ecogia 16, 1290 Versoix, Switzerland
[12] *Herschel*/*Planck* Project, Scientific Projects Dpt of ESA, Keplerlaan 1, 2200 AG, Noordwijk, The Netherlands
[13] IFP-CNR, Istituto di Fisica del Plasma, Consiglio Nazionale delle Ricerche, via Roberto Cozzi, 53, 20125 Milano, Italy
[14] Jodrell Bank Centre for Astrophysics, University of Manchester, M13 9PL, UK
[15] ASI, Agenzia Spaziale Italiana, Viale Liegi, 26, 00198 Roma, Italy
[16] Dipartimento di Fisica, Università di Trieste, via A. Valerio n. 2, 34127 Trieste, Italy
[17] Instituto de Fisica de Cantabria, CSIC- Universidad de Cantabria, Avenida de los Castros s/n, 39005 Santander, Spain
[18] Instituto de Astrofísica de Canarias, C/ vía Láctea s/n, 38200, La Laguna, Tenerife, Spain
[19] University of Helsinki, Department of Physics, PO Box 64, 00014 Helsinki, Finland
[20] Metsähovi Radio Observatory, TKK, Helsinki University of Technology, Metsähovintie 114, 02540 Kylmälä, Finland
[21] Physics Department, University of California, Santa Barbara, CA 93106, USA
[22] Institute of Theoretical Astrophysics, University of Oslo, PO Box 1029 Blindern, 0315 Oslo, Norway

[23] Centre of Mathematics for Applications, University of Oslo, PO Box 1053 Blindern, 0316 Oslo, Norway
[24] ESA/ESAC/RSSD, European Space Agency, European Space Astronomy Centre, Research and Scientific Support Department, PO Box – Apdo. de correos 78, 28691 Villanueva de la Cañada, Madrid, Spain
[25] Osservatorio Astrofisico di Arcetri, L.go E. Fermi 5, Firenze, Italy
[26] Department of Astronomy, Haverford College, Haverford, PA 19041, USA
[27] Research and Scientific Support Department of ESA, ESTEC, Keplerlaan 1, 2201 AZ Noordwijk, The Netherlands
[28] Institute for Space Sciences, Bucharest-Magurele, Str. Atomostilor, 409, Po Box Mg-23, Ro-077125, Romania
[29] Lawrence Berkeley National Laboratory and Berkeley Center for Cosmological Physics, Physics Department, University of California, Berkeley CA 94720, USA
[30] Department of Physics and Astronomy, University of British Columbia, Vancouver, BC, V6T 1Z1, Canada
[31] University of Oxford, Astrophysics, Keble Road, Oxford, OX1 3RH, UK
[32] Université Paris 7, APC, Case 7020, 75205 Paris Cedex 13, France
[33] MilliLab, VTT Technical Research Centre of Finland, Information Technology PO Box 1000, 02044 VTT, Finland
[34] Helsinki Institute of Physics, PO Box 64, 00014 Helsinki, Finland
[35] INAF-OABo, Istituto Nazionale di Astrofisica, Osservatorio Astronomico di Bologna, via Ranzani 1, 40127 Bologna, Italy
[36] INFN, Istituto Nazionale di Fisica Nucleare, Sezione di Trieste, via Valerio, 2, 34127 Trieste, Italy
[37] INFN, Istituto Nazionale di Fisica Nucleare, Sezione di Tor Vergata, via della Ricerca Scientifica 1, 00133 Roma, Italy
[38] University of California, Berkeley Space Sciences Lab 7 Gauss Way Berkeley, CA 94720, USA
[39] Computational Cosmology Center, Lawrence Berkeley National Laboratory, Berkeley CA 94720, USA
[40] CESR, Centre d'Étude Spatiale des Rayonnements, 9 Av du Colonel Roche, BP 44346, 31028 Toulouse Cedex 4, France
[41] ESA – ESAC, European Space Agency, European Space Astronomy Centre, Villafranca del Castillo, Apdo. 50727, 28080 Madrid, Spain
[42] Warsaw University Observatory, Aleje Ujazdowskie 4, 00-478 Warszawa, Poland
[43] Astrophysics Group, Cavendish Laboratory, J.J. Thomson Avenue, CB3 0HE, Cambridge, UK
[44] Department of Physics, University of Miami, 1320 Campo Sano Avenue, Coral Gables, FL 33124, USA
[45] ASI, Agenzia Spaziale Italiana, Science Data Center, c/o ESRIN, via G. Galilei, 00044 Frascati, Italy
[46] Dipartimento di Fisica, Università di Roma "La Sapienza", p.le A. Moro 2, 00185 Roma, Italy
[47] INAF-OARo, Istituto Nazionale di Astrofisica, Osservatorio Astronomico di Roma, via di Frascati 33, 00040 Monte Porzio Catone, Italy
[48] Istituto di Scienza e Technologie dellInformazione "Alessandro Faedo", CNR, Consiglio Nazionale delle Ricerche, Area della Ricerca di Pisa, via G. Moruzzi 1, 56124 Pisa, Italy
[49] Department of Physics and Astronomy, University of California Berkeley, CA 94720, USA